NIST Grant/Contractor Report
NIST GCR 24-053

# Research on Fixture-Level Peak Probability of Water Use in Commercial Buildings

Steven Buchberger
Tao Li
Toritseju Omaghomi
Gary Klein

This publication is available free of charge from:
https://doi.org/10.6028/NIST.GCR.24-053

NATIONAL INSTITUTE OF STANDARDS AND TECHNOLOGY
U.S. DEPARTMENT OF COMMERCE

NIST Grant/Contractor Report
NIST GCR 24-053

# Research on Fixture-Level Peak Probability of Water Use in Commercial Buildings

Steven Buchberger
Tao Li
Toritseju Omaghomi
*University of Cincinnati*

Gary Klein
*Gary Klein Associates*

This publication is available free of charge from:
https://doi.org/10.6028/NIST.GCR.24-053

June 2024

U.S. Department of Commerce
*Gina M. Raimondo, Secretary*

National Institute of Standards and Technology
*Laurie E. Locascio, NIST Director and Under Secretary of Commerce for Standards and Technology*

NIST GCR 24-053
June 2024



This publication was produced as part of cooperative agreement 70NANB21H181 with the National Institute of Standards and Technology. The contents of this publication do not necessarily reflect the views or policies of the National Institute of Standards and Technology or the US Government.

**NIST Technical Series Policies**


**How to Cite this NIST Technical Series Publication**
Buchberger S, Li T, Omaghomi T, Klein G (2024) Research on Fixture-Level Peak Probability of Use in Commercial Buildings. (National Institute of Standards and Technology, Gaithersburg, MD), NIST Grant/Contractor Report (GCR) NIST GCR 24-053. https://doi.org/10.6028/NIST.GCR.24-054

**Abstract**

A novel wireless sensor network is developed and demonstrated for monitoring indoor fixture level water use in buildings. The new technology consists of a low-cost, battery-powered, miniature wireless sensor module for non-invasive detection of flow through pipes. When deployed in a typical commercial, industrial, or residential building, the modules form a remote wireless sensor network that accurately monitors the incidence and patterns of water usage at individual fixtures. As proof of concept, the wireless sensor network was deployed and tested in a dormitory at the University of Cincinnati (UC) where several water fixtures were monitored at a 1-second interval for a period of five months. The water use data were analyzed to obtain peak period probabilities of fixture use (*i.e.*, *p*-values). Fixture *p*-values are needed to estimate the instantaneous peak water demand in buildings, the key parameter for properly sizing premise plumbing systems. A dimensionless ramp function on the unit square is developed and demonstrated as a versatile approach to help engineers obtain reasonable estimates of fixture *p*-values in new buildings where water use data may be lacking or sparse. A protocol is suggested to guide investigators on how to compile, consolidate, and archive high resolution water use data into a cloud-based repository. Results include preliminary estimates of *p*-values for restroom fixtures in a large sports arena on the UC campus. Peak flows at the sport arena measured during five NCAA basketball game days are compared against predicted peak flows from the Water Demand Calculator. Finally, peak flow measurements at 20 large contemporary residential buildings across the US are compared against predictions of the 99$^{th}$ percentile from the Water Demand Calculator.

**Keywords**

Commercial Buildings; Fixture Probability; Peak Water Demand; Wireless Sensor; Water Demand Calculator.

## Table of Contents

## List of Tables



## List of Figures

# 1. Introduction

Instantaneous peak water demand is an important consideration when designing a new building or repurposing an existing structure. The peak water demand affects the scale and cost of the entire premise plumbing system, including meter size, heater capacity, pipe diameters, valves, and other related hydraulic appurtenances. Determining the peak water demand is challenging because instantaneous water use in a building is difficult to predict. The diurnal water use pattern never repeats exactly, and, as a consequence, the magnitude of the peak demand varies randomly from day to day.

This problem was first investigated nearly 100 years ago by Dr. Roy Hunter, a research physicist at the National Bureau of Standards. Recognizing that water use is a random process, Hunter applied probability principles to estimate peak water demand based on the total number of fixtures in a building and on the flow drawn when a fixture is operated. The peak demand determines the size of the service line and many other features of the premise plumbing system.

Hunter's crowning achievement was the development of a design graph known as "Hunter's Curve", which gives the 99th percentile water demand versus total fixture units for any combination of indoor end uses [1]. Hunter did not attempt to predict the absolute maximum possible water demand. Instead, he defined a threshold for design so that there is only a 1 % chance that the actual peak period demand will exceed the load estimated from his curve.

Hunter's iconic curve is an ingenious blend of theoretical rigor and practical simplicity. It quickly became the basis for plumbing codes in the United States and across the globe [2]. Hunter's work established the standard for satisfactory service of building water supply systems. The problem, however, is that Hunter's curve is frozen in time; it is a snapshot of peak indoor water use in 1940.

In recent years, a growing consensus has emerged among practicing engineers that Hunter's curve leads to overdesign of the premise plumbing system in new buildings [3,4,5]. There are a couple of reasons for this. First, Hunter's assumption of congested service (*i.e.*, users form a queue at fixtures) often does not hold. Second, flow rates based on plumbing fixtures from the 1930s do not apply to the new generation of water-conserving fixtures, especially those imposed by the passage of the 1992 Energy Policy Act (EPAct) and subsequent green plumbing codes.

There have been many attempts to salvage Hunter's curve by tweaking fixture-unit values for contemporary end-use applications. Often these modifications reflect engineering judgment rather than observable data. These ad hoc adjustments have led to discrepancies among fixture-unit values posted in various plumbing codes [6].

In 2011, the International Association of Plumbing and Mechanical Officials (IAPMO), the American Society of Plumbing Engineers (ASPE), and the University of Cincinnati (UC), in collaboration with the Water Quality Association (WQA), convened a task group to review methods for estimating peak demands in buildings fitted with water-conserving fixtures.

The task group acquired a large database of high-resolution indoor water use measurements taken between 1996 and 2011 at nearly 1100 single-family homes in 62 cities across the United States [7]. Because the dataset provided statistics only for residential end use, the scope of work was narrowed to single and multi-family residential dwellings. Residential indoor fixtures considered in the database were bathtubs, showers, dishwashers, clothes washers, faucets, and toilets.

The task group was charged with developing a probability model to predict the peak water demand for single- and multi-family dwellings having water-conserving plumbing fixtures. In other words, the goal was to bring Hunter's curve into the 21st century. Not surprisingly, analysis of the modern residential database led to several significant changes in the parameters of the binomial probability model that underpins Hunter's method. Most notably, for tank toilets, the probability that the fixture is drawing water during the peak hour dropped from 20 % to 1 %, and the fixture flow rate decreased from 15 Liters Per Minute (LPM) to 11 LPM (4 Gallons Per Minute [GPM] to 3 GPM) [8]. A complete listing of all recalibrated parameter values for water-conserving residential fixtures is available in the summary report [7].

Rather than create a new design curve that essentially would be a snapshot of peak water use in 2020, the task group opted to employ a digital-age resource. Keeping with the spirit of Hunter's probabilistic approach, a set of three algorithms was coded into a user-friendly spreadsheet called the Water Demand Calculator (WDC). The user provides the itemized fixture count for their residential building. Then, armed with information about the probability of fixture use and flow of an operating fixture (the *p* and *q* values, respectively), the WDC computes the 99th percentile of the peak period water demand. The WDC program is available at no charge from the IAPMO website. Fig. 1 shows the WDC input template and computed results for a multi-family building with ten apartments.

For single-family homes, where the total fixture count is generally under 30, the WDC uses exhaustive enumeration (ExEn) to delineate all possible water use combinations. While offering an exact solution, ExEn carries a high computational burden. For instance, in a home with 15 fixtures, ExEn involves $2^{15}$ or 32 768 calculations. For large residential buildings with hundreds of fixtures, ExEn is intractable. In this case, the WDC estimates the 99th percentile of the water demand using the normal approximation to the Poisson-binomial distribution, as first proposed by ASPE engineer Robert Wistort [9]. Between these household extremes, the WDC uses a new modified Wistort method to predict peak demands in the transition region from single-family homes to large residential buildings. Recently, a convolution-based algorithm suggested by Herbert [10] has been investigated and coded into the WDC as a computational option for buildings with fixture counts under 40. Preliminary testing suggests that the convolution approach can reduce the run time compared to the existing exhaustive enumeration scheme.

Extensive beta testing of the WDC at several large residential locations across the United States and Australia has yielded very reasonable results. Based on this encouraging performance, the WDC has been incorporated into Appendix M of the Uniform Plumbing Code [11, 12]. With the impending release of the fourth edition of the M22 Manual of Water Supply Practice [13], the WDC has been endorsed by the American Water Works Association (AWWA) as the preferred method for estimating peak indoor water demands in all residential buildings.

Like Hunter's seminal work from 1940, the theoretical basis for the WDC has a rock-solid foundation. With proof of concept clearly demonstrated, the framework for the WDC is poised to serve as a design aid for estimating peak demands in non-residential buildings. To extend the WDC to the non-residential sector, one major hurdle remains: there is a need to assemble and analyze a national database of water use measurements from buildings in the non-residential sector, as outlined in the recent NIST report on research needs for premise plumbing systems [14]. This critical step is essential to estimate values for the probability of fixture use, the elusive "*p*-values" that lie at the heart of Hunter's curve and the WDC.

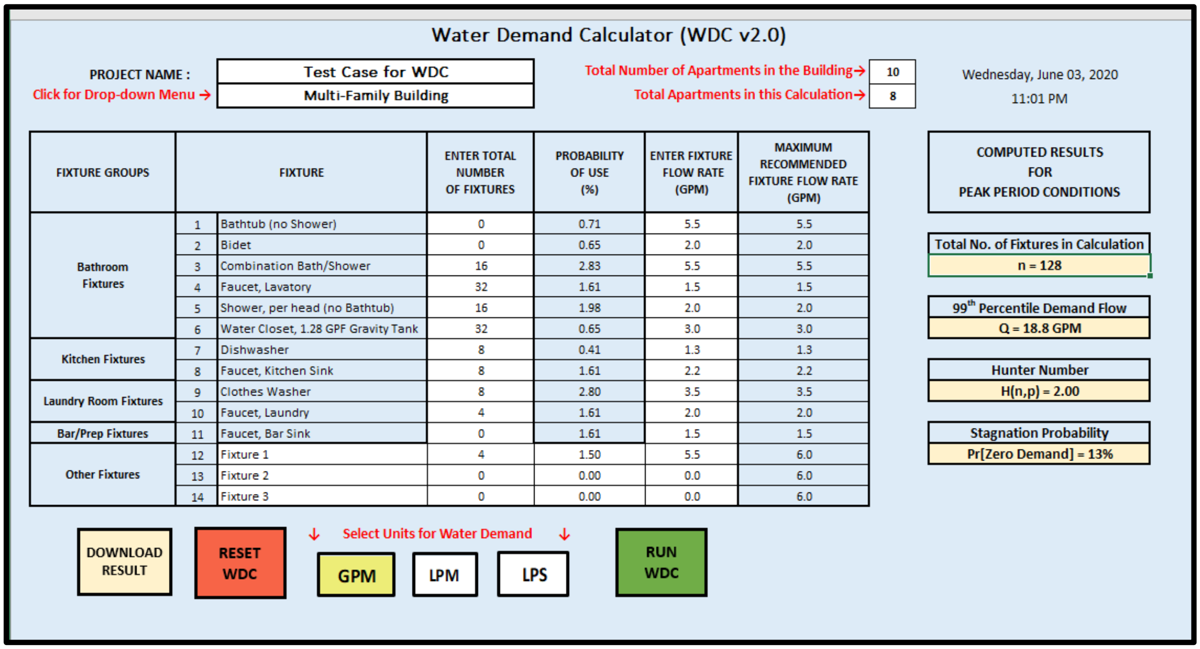
Water Demand Calculator (WDC v2.0)

PROJECT NAME : Test Case for WDC
Click for Drop-down Menu → Multi-Family Building
Total Number of Apartments in the Building→ 10
Total Apartments in this Calculation→ 8
Wednesday, June 03, 2020
11:01 PM

| FIXTURE GROUPS | | FIXTURE | ENTER TOTAL NUMBER OF FIXTURES | PROBABILITY OF USE (%) | ENTER FIXTURE FLOW RATE (GPM) | MAXIMUM RECOMMENDED FIXTURE FLOW RATE (GPM) |
|---|---|---|---|---|---|---|
| Bathroom Fixtures | 1 | Bathtub (no Shower) | 0 | 0.71 | 5.5 | 5.5 |
| | 2 | Bidet | 0 | 0.65 | 2.0 | 2.0 |
| | 3 | Combination Bath/Shower | 16 | 2.83 | 5.5 | 5.5 |
| | 4 | Faucet, Lavatory | 32 | 1.61 | 1.5 | 1.5 |
| | 5 | Shower, per head (no Bathtub) | 16 | 1.98 | 2.0 | 2.0 |
| | 6 | Water Closet, 1.28 GPF Gravity Tank | 32 | 0.65 | 3.0 | 3.0 |
| Kitchen Fixtures | 7 | Dishwasher | 8 | 0.41 | 1.3 | 1.3 |
| | 8 | Faucet, Kitchen Sink | 8 | 1.61 | 2.2 | 2.2 |
| Laundry Room Fixtures | 9 | Clothes Washer | 8 | 2.80 | 3.5 | 3.5 |
| | 10 | Faucet, Laundry | 4 | 1.61 | 2.0 | 2.0 |
| Bar/Prep Fixtures | 11 | Faucet, Bar Sink | 0 | 1.61 | 1.5 | 1.5 |
| Other Fixtures | 12 | Fixture 1 | 4 | 1.50 | 5.5 | 6.0 |
| | 13 | Fixture 2 | 0 | 0.00 | 0.0 | 6.0 |
| | 14 | Fixture 3 | 0 | 0.00 | 0.0 | 6.0 |

COMPUTED RESULTS FOR PEAK PERIOD CONDITIONS
Total No. of Fixtures in Calculation
n = 128
99th Percentile Demand Flow
Q = 18.8 GPM
Hunter Number
H(n,p) = 2.00
Stagnation Probability
Pr[Zero Demand] = 13%

DOWNLOAD RESULT
RESET WDC
Select Units for Water Demand
GPM
LPM
LPS
RUN WDC

**Fig. 1.** Input Template for the Water Demand Calculator.

## 2. Research Objectives

The current version of WDC is limited to residential buildings because the data used to estimate the fixture use parameters came solely from the residential sector. Given the pressing need to estimate the fixture parameters for non-residential buildings in the US and, in doing so, extend the WDC to commercial and institutional buildings, the research project described in this report had three main objectives:

**Objective 1 – Data Collection Using a Wireless Sensor Network:** Deploy water sensor devices in a commercial building in the Cincinnati metro area. Test the wireless sensor network to accurately and reliably monitor and record continuous high-resolution fixture-level water use in the select building. Compile signals from the sensor network in a unique database for subsequent analysis and estimation of the peak hour probabilities of fixture use (*i.e.*, the fixture *p*-values).

**Objective 2 – Data Analysis:** Develop and demonstrate an efficient minimum variance statistical procedure for estimating the probability of fixture operation from the water use database collected via the wireless sensor network. The parameters of interest include hourly arrival rates, service rates, building water use patterns, and the peak period fixture *p*-values.

**Objective 3 – Data Archiving:** Develop and implement a reliable, robust, convenient, and secure protocol for screening, formatting, storing, and accessing the fixture-level water use data collected on the wireless sensor network. The raw data collected will be among the first in a national database of water use characteristics for commercial buildings with public access.

# 3. Task 1: Develop Wireless Distributed Network for Monitoring Fixture Use in Premise Plumbing System

## 3.1. Overall System

The objective of this task is to develop and test a novel, low-cost, battery-powered, miniature wireless sensor module for non-invasive detection of flow through pipes in premise plumbing systems (Fig. 2). When deployed in a typical commercial, industrial, or residential building, the modules will form a wireless sensor network to accurately monitor the incidence and patterns of water usage at various fixtures. Readings from this sensor network can be analyzed to estimate the peak hour *p*-values for various fixtures in the premise plumbing system, hence providing a sound basis to apply the promising new method for estimating peak indoor water demand.

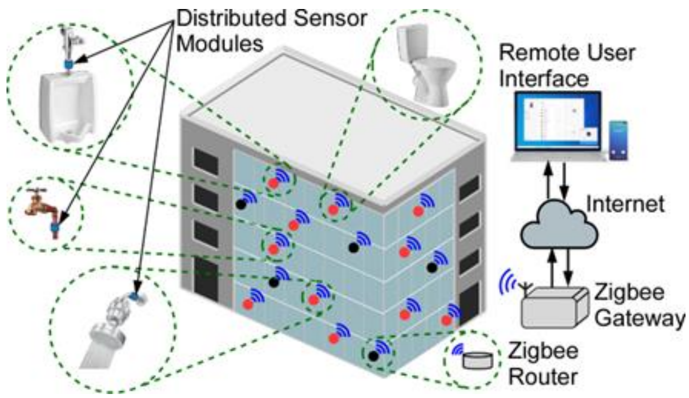


**Fig. 2.** System Concept Design.

As illustrated in Fig. 2, the wireless sensor network system is based on the Zigbee protocol. It consists of a group of miniature sensor modules, several Zigbee routers, and a Zigbee gateway. The sensor module is battery-powered for direct attachment to waterpipes without any cable or external power sources. Therefore, it can be distributed in a building under investigation at strategically selected sites for various types of plumbing fixtures. The Zigbee routers were deployed to help expand the coverage range of the Zigbee network as necessary. The Zigbee gateway consists of a Zigbee coordinator and a Raspberry Pi unit. The coordinator interfaces with sensor modules and Zigbee routers with time synchronization among all units to ensure proper timestamp recording. The Raspberry Pi provides functions including system control, data collection and management, interface with the Internet for data storage/backup in the cloud, and remote interaction with end users through web applications.

## 3.2. Sensor Module Design

### 3.2.1. Overall Design of Sensor Module

The proposed design of each sensor module in the wireless sensor network is illustrated in Fig. 3. The sensor module includes a non-invasive flow sensor unit, a microcontroller (MCU) with an embedded transceiver for wireless communication based on a low-power protocol called Zigbee, and a replaceable battery along with the power regulation circuit. The flow sensor unit combines two sensor modalities. The acoustic measurement using a microphone is defined as sensor modality 1 (SM1), and a thermal detection based on heater and temperature readers is defined as sensor modality 2 (SM2). SM1 and SM2 were implemented in the sensor module to form a hybrid detection to achieve high accuracy and fast response time.

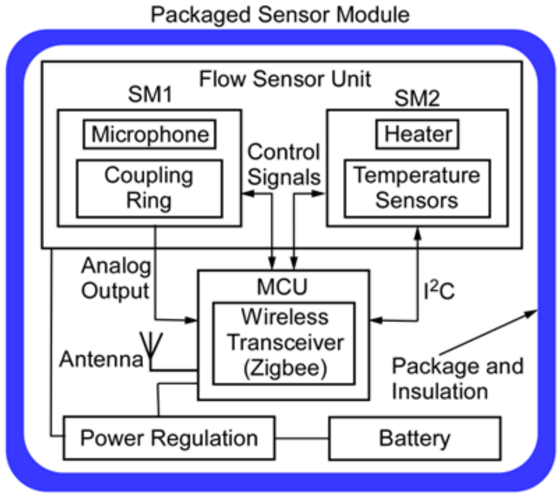


**Fig. 3.** Sensor Module Diagram.

### 3.2.2. Sensor Modality 1

#### 3.2.2.1. SM1 Architecture

In the SM1, the acoustic detection will be done using a high-sensitivity miniature microphone chip, which can almost instantaneously detect the water flow on/off events.

In this effort, we initially investigated a commercial analog Microelectromechanical Systems (MEMS) microphone with an ultralow power consumption and high signal-to-noise ratio (or SNR) of 60.5 and a size of only 3.76 mm x 2.95 mm x 1.3 mm. An essential feature of this chip is that it can continuously monitor the surrounding sound in sleep mode with low power consumption and send a triggering signal to wake up the MCU when the sound level exceeds a predefined threshold. However, through initial experimental evaluation, we observed that this microphone could not consistently pick up water flow sounds at one of the field test sites, likely due to limited sensitivity. Therefore, we switched to an alternate digital microphone which has higher sensitivity. This is a MEMS digital microphone with a sensitivity of -26 dBV (compared to -38 dBV of the analog microphone), low power consumption, high SNR of 65, and a size of only 3.5 mm x 2.65 mm x 0.98 mm. The MCU remains active and records sound data from the microphone every 0.5 s. An algorithm processes the recorded data. This algorithm includes signal filtering for the removal of noise and interference components. It also includes calculating a signal strength parameter to compare with a threshold that the experiments will determine. If the sound exceeds the pre-set threshold value, it indicates there is water flow, and MCU will turn on SM2; otherwise, the MCU and microphone will go back to sleep mode.

### 3.2.2.2. Figure of Merit for Detection Algorithm

The water flow detection algorithm comprises of two parts, *i.e.*, use of a digital filter and a function to calculate a dimensionless signal strength indicator (SSI) function. In the process to develop the SM1 algorithm, a custom-defined Figure of Merit (FoM) is developed to quantitatively evaluate the effectiveness of different algorithms to differentiate between the water flow sound and noise. This is given as the detection algorithm output of water flow sound divided by the algorithm output of noise signals which can be a normal average or weighted average of different types of noises, as shown in the equation below. Higher FoM indicates a stronger capability of the algorithm to differentiate water flow sound from noise.

$$Figure\,of\,merit = \frac{R(Water\ flow)}{A_1R(Noise_1) + A_2R(Noise_2) + ... + A_nR(Noise_n)}$$

where *R (Water flow/Noise)* is an output of the detection algorithm applied to water flow sound only or noise only, and $A_1$, $A_2$...$A_n$ are weighting factors of different noise types.

Three candidates were considered for the signal strength indicator function: RMS (power), energy, and amplitude. Table 1 defines and compares these three potential candidates, including a mathematical representation of each function.

**Table 1.** Comparison of Candidate Methods for Signal Strength Indicator Functions.

| RMS (Power) | Energy | Amplitude |
|---|---|---|
| 1. Measures the power of a signal | 1. Measure the energy of a signal | 1. Measures the amplitude of a signal (sum of absolute values) |
| 2. $R\_rms(x) = \frac{1}{n}\sum_{k=1}^{n} x(n)_k^2$ | 2. $R\_eng(x) = \sum_{n=0}^{N} \lvert x(n) \rvert^2$ | 2. $R\_amp(x) = \sum_{n=0}^{N} \lvert x(n) \rvert$ |

### 3.2.2.3. Algorithm Design and Evaluation

a) Selection of Filter

The digital filter removes the undesired noise signals while keeping the water flow sound in the recorded sound. The general criteria for selecting the filters for our application are as follows:

i. Cutoff frequencies are chosen to remove undesired frequency components of noise as much as possible (filters with steeper roll-off rates are preferred).

ii. Less memory requirement (depending on type and order of the filter, lower order typically means smaller memory needed).

iii. High computational efficiency (less computing power required).

Criteria ii and iii are essential to allow the filter to be feasible for implementation with a microcontroller with an ARM processor with limited memory size and computing capability. After carefully considering different filter classes, IIR filter class was selected because it is more suited for the application and should allow easier implementation.

IIR filter type consists of mainly 4 filters: Butterworth, Chebyshev type I, Elliptical, and Bessel. The elliptical filter is chosen as the initial choice for our application, given its steepest roll-off between the passband and stopband of the filter spectrum. However, the elliptical filter is also the most complicated and challenging to implement, given the MCUs limited computing power and memory size. Further, Chebyshev (Type I) and Butterworth filters don't have as steep roll-off rates as an elliptical filter but are still acceptable and will be considered in further tests to evaluate their effects considering they are expected to be easier to implement in the MCU.

b) Determination of Filter Cutoff Frequencies

As filters' most important design parameter, cutoff frequencies separate the passband and stopband. We evaluated the effect of cutoff frequency on the capability to differentiate between water flow sounds and noises.

In this evaluation, FoM was calculated using normalized water flow sound and common noises while the filter cutoff frequency was swept for each signal strength indicator function. After evaluation, it was identified that the higher values of FoM lie between approximately 1.5 kHz to 3.2 kHz, which suggests that water flow sound dominates in that frequency range above the cutoff frequency compared to noise signals. However, the types of noises being considered will still affect the cutoff frequency. We considered 7 types of noises in this analysis and will consider other types for more thorough evaluations, particularly those recorded from realistic scenarios in the target deployment sites for field tests.

#### 3.2.2.4. Enhanced Algorithm for Water Flow Detection with Digital Microphone

During field tests, the new microphone with higher sensitivity could record the water flow sound that can then be used to detect water flow events. However, due to the higher sensitivity, a few new types of interference sounds were picked up in the recording in addition to the water flow sound through the pipe. These interferences include toilet flushes, door opening and closing sounds, and a periodic interference that lasts 6s each and occurs every 30s only when the monitoring location (a restaurant in a college dormitory) is in operation. Further enhancements were made to the initial algorithm, including fine adjustment of filter cutoff frequency and other new post-filtering steps.

#### 3.2.2.5. SM1 Microphone Integration

The acoustic port on the bottom of the microphone chip is aligned with a through hole on the fabricated PCB with a solder ring. This is demonstrated in Fig. 4. The silicone coupling ring is used to properly mount the PCB to the surface of the water pipe, forming an acoustic chamber that helps collect sound and enhance the acoustic coupling between the waterpipe and the microphone chip while minimizing interference from the exterior noise. Another layer of insulation material is wrapped outside the sensor module PCB to reduce the noise interference further while also providing thermal isolation for the SM2 thermal detection approach.

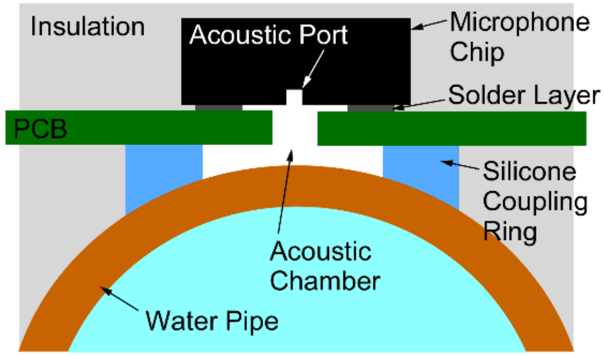


**Fig. 4.** SM1 Microphone Integration.

### 3.2.3. Sensor Modality 2

#### 3.2.3.1. Detection Principle

Sensor modality 2 (SM2) is based on the calorimetric thermal flow sensing method, as illustrated in Fig. 5. Two temperature sensors are placed symmetrically beside a heating element, one on the upstream side (T1) and the other on the downstream side (T2). When there is no flow, the temperature gradient created by the heater is symmetrical, and the temperature sensors generate readouts T1=T2.

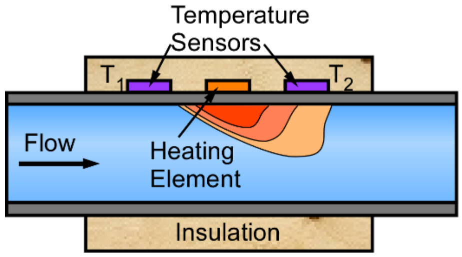


**Fig. 5.** Calorimetric Thermal Flow Sensing Method.

When there is flow, the temperature gradient is disturbed, causing T2>T1. The temperature difference ΔT=T2-T1>0 indicates the presence of the flow, and its value correlates with the flow rate. Using a heater and temperature sensors of a few mm in size and embedding both on a small PCB, the thermal flow sensor can be made with a compact footprint to improve the detection sensitivity and reduce the power consumption. This thermal technique can potentially provide flow rate information, although it will have a slower response time than SM1.

#### 3.2.3.2. SM2 Design

In the design of the PCB for SM2, multiple designs have been considered, with the temperature sensors placed at a distance L from the heater. L was varied in different designs of the PCB to evaluate its effect on flow detection; its optimization is described in Sec. 3.2.3.4. Multiple open slots around the temperature sensors are included to provide thermal isolation from the rest of the PCB to help reduce thermal conductance. The symmetric placement of the upstream and downstream temperature sensors with respect to the heater is essential to minimize the offset in the readings from the two sensors. The center slot on the PCB is used to align the heater centrally between the two temperature sensors. The fabricated PCB was assembled with all components (Fig. 6) using our in-house SMD reflow process.

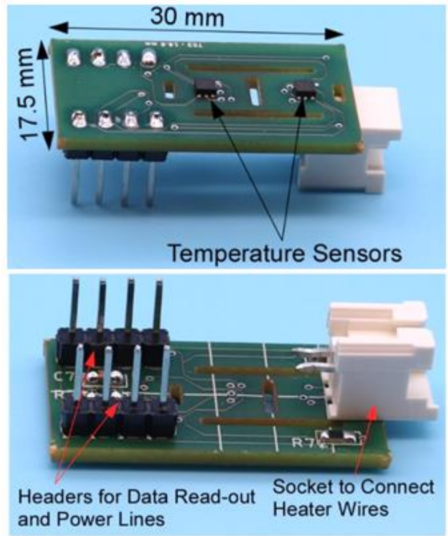


**Fig. 6.** Assembled PCB: Top side (Top), Bottom side (Bottom).

A high-resistivity nichrome wire is used as the heating element. The nichrome wire is coiled around a 3D-printed heater holder to form the heater. The heater holder is designed to fit in the center slot of the PCB. An in-house precision wire winding machine was built to precisely wind the nichrome wire on the heater holder.

### 3.2.3.3. Holder for Both SM2 PCB and Heater

When the heater holder was placed directly in the center slot on the SM2 PCB, as done in an initial design, heat could be transmitted directly from the heater coil through the PCB to the temperature sensors, according to results from extensive testing. Moreover, a better approach was required to place the PCB and the heater on the water pipe for easier integration of the system on the water pipe. Considering these 2 aspects, we came up with a new two-part design of the holder (Fig. 7) for both the PCB and the heater. The holder can be manufactured using 3D-printing and, if large volume production is required, through injection molding. Inside this holder, we have features to allow accurate placement of the PCB on the holder and a bridge to be used as the heater holder. This bridge structure has a place for the heater wire to be wound and placed in the recesses on the holder without directly touching the PCB, thus eliminating the direct heat conduction path from the heater coil to the temperature sensors.

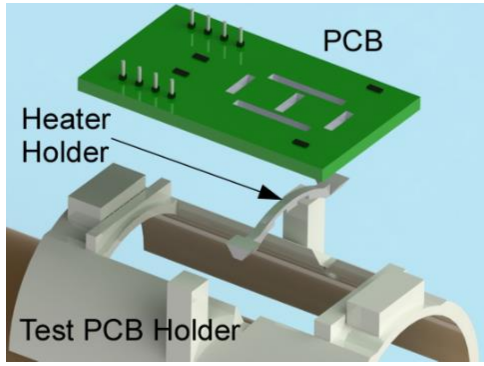


**Fig. 7.** Holder Design.

The holder has a pair of recesses to integrate the heater holder and 4 guideposts to allow the PCB to sit accurately. Figure 8 shows an assembled SM2 test device after integrating the heater holder, an SM2 test PCB, and the PCB holder. To print these parts, the on-campus 3D printing service was used.

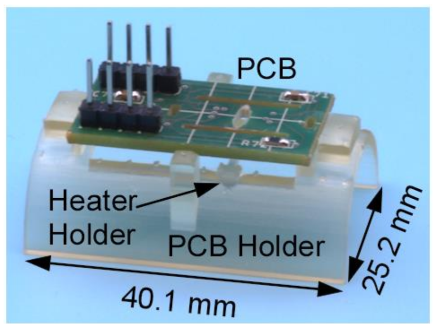


**Fig. 8.** Assembled Test PCB for SM2 on PCB Holder.

### 3.2.3.4. Holder for Both SM2 PCB and Heater

The distance L between the heater and each of the symmetric T1 and T2 temperature sensors is a critical design parameter that affects the thermal coupling efficiency through the wall of the copper pipe with the water. Simulations were performed for a series of L values to find the maximum $\Delta T$ between the two temperature sensors in the presence of water flow, as the largest $\Delta T$ indicates maximum thermal coupling between the heater and water through the thickness of the waterpipe. Figure 9 shows the simulation model on a ¾" copper waterpipe with a flow rate of 0.315 L/s (5 GPM) used for optimization in COMSOL® Multiphysics. Figure 10 plots the temperature difference $\Delta T$ at different L values. As shown with the blue dots, the optimal L was ≈12mm. This was compared with experimental optimization results described later in Sec. 3.4.

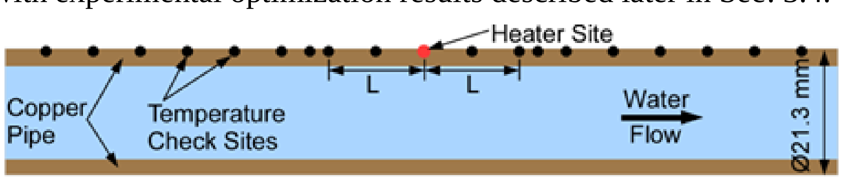


**Fig. 9.** Simulation Model for Heater-Sensor Distance Optimization.

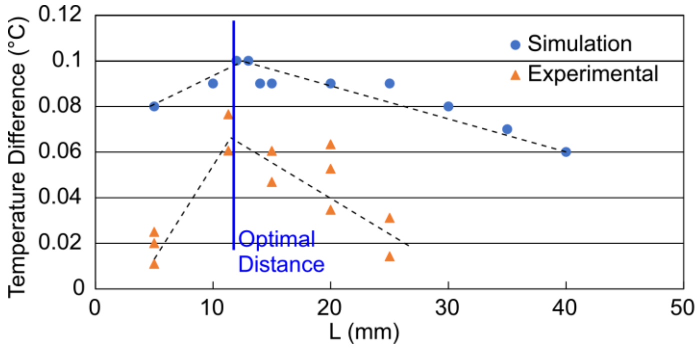


**Fig. 10.** Comparison of L Optimization Results from Simulation and Experiments.

### 3.2.4. Sensor Module Packaging

To facilitate the installation of the sensor modules on the water pipe at the test sites, we designed a sensor module package that integrates the various components of the module. The package's appearance is shown in Fig.11. This package can be used to integrate all the elements of the system module, including the power source, the power bank, the main PCB, the SM2 plug-in PCB as well as the other components that can allow the PCB to sit on the water pipe properly. The components within the package, including the power bank, coupling ring, heater, and PCBs, are shown in Fig. 12. There is still space within the package that can be optimized further to reduce the size of the overall packaged sensor module. Currently, the size of the package is 12 cm x 8.1 cm x 6.4 cm.

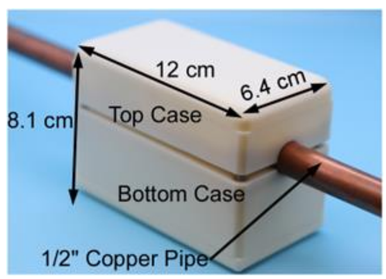


**Fig. 11.** Sensor Module Package (Outside).

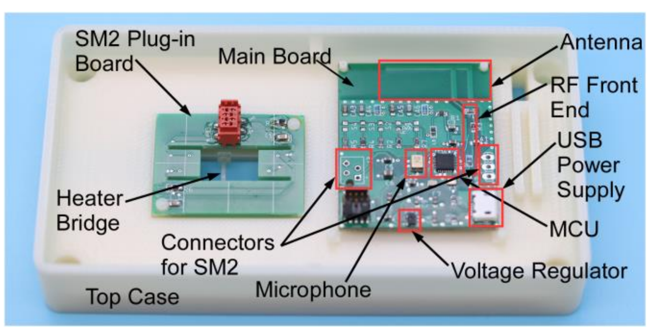


**Fig. 12.** Sensor Module Package (Inside).

### 3.2.5. Preparation of Test Device for Stage 1 of the Two-Stage Field Test

A two-stage field test plan has been designed to evaluate the sensor module under development. Stage 1 will collect realistic sound data, including water flow and noise, for training and further testing the SM1 algorithm, and stage 2 will test the whole sensor module and wireless sensor network. The following sections describe the preparation of a test device for the Stage 1 field test.

a) Device Configuration for Stage 1 Testing

Figure 13 shows the configuration of the test device used for the Stage 1 field test. The test device includes a microphone, MCU, and Raspberry Pi, which is a credit card-sized computer module. All these components are connected with wired connections. This test device was mounted on a water pipe at the test site in the same way as planned for a real sensor module.

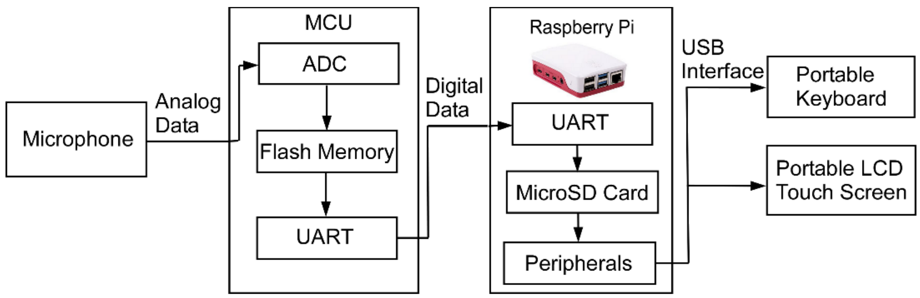


**Fig. 13.** Functional Block Diagram for Device Configuration for Stage 1 Testing Using an Analog Microphone.

Initial tests were performed using the analog microphone (Fig. 13). However, as mentioned earlier, an issue with the consistency of using the analog microphone was identified during initial testing at one of the field test sites. Hence, the analog microphone was replaced with an alternate digital microphone with higher sensitivity. Figure 14 shows the updated functional block diagram for later stage 1 field tests.

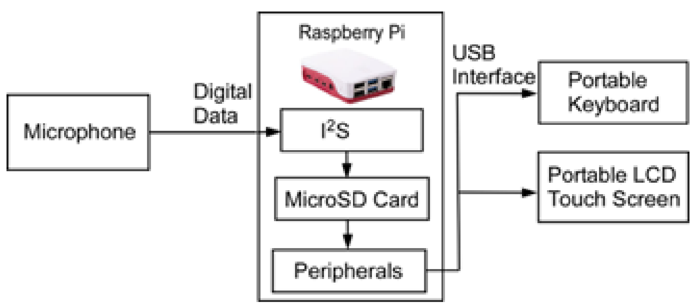


**Fig. 14.** Functional Block Diagram for Device Configuration for Stage 1 Testing Using Digital Microphone.

b) Stage 1 Test Setup

Figure 15 shows the photo of the Stage 1 field test system, including all components. The figure displays the SM1 test PCB, Raspberry Pi with a transparent case and a size similar to a credit card, and a portable touch screen that can be used for field operation of the system for test initiation, etc. The portable keyboard can also be connected if necessary, or the touch screen can be used to control. A portable battery is also connected to power the test PCB and Raspberry Pi, as well as the touch screen and other components when they are used.

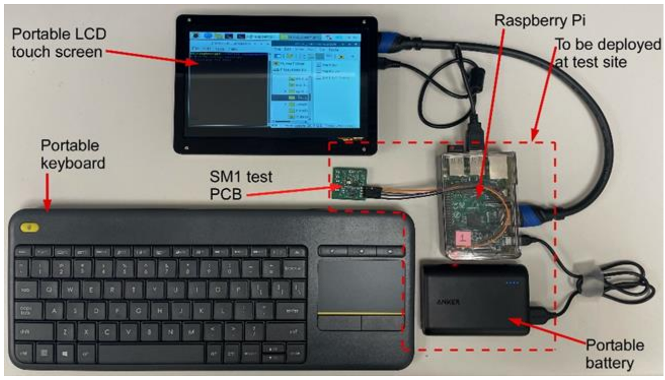


**Fig. 15.** Stage 1 Test Setup.

The components inside the red dashed line box were deployed and left at the test site using adhesive tape or other means to secure them to the water pipe. The image does not show the fiberglass insulation, which will be used to provide additional noise attenuation as necessary.

### 3.2.6. Sensor Module Circuit Design and Fabrication

Figure 16 shows the overall circuit schematic diagram for the design of the integrated sensor module. We are using two separate PCBs: one is referred to as the main PCB that consists of the MCU, the RF front end including the antenna for the wireless communication through the Zigbee network, the microphone that has the SM1 sensor modality, and the heater driver, which is for SM2 to control the power delivered to the heater. Furthermore, the power source circuit converts the 5 V from a USB power bank to 3.3 V, using voltage regulators to support components on the PCB.

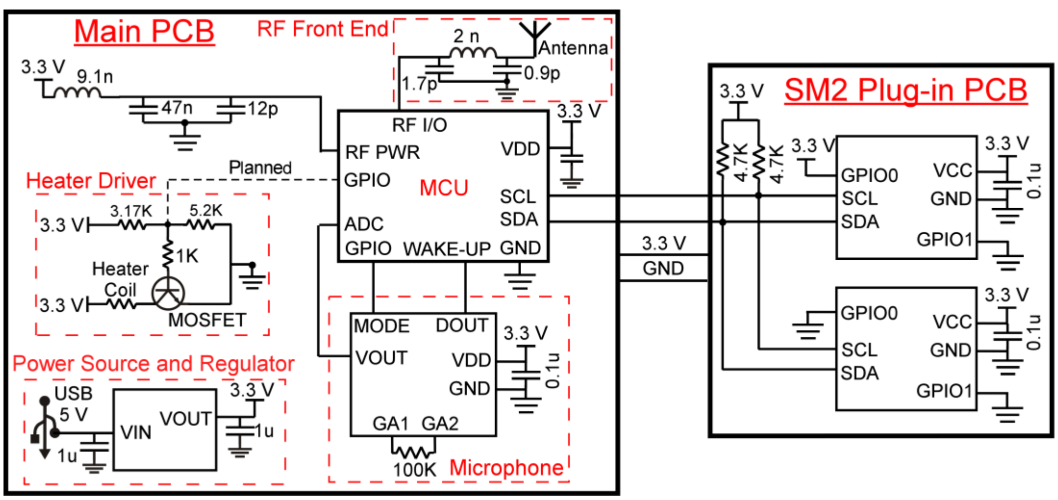


**Fig. 16.** Schematic of Sensor Module Circuit Diagram.

Figure 17 shows the fabricated main PCB based on the circuit diagram schematic. We used the inverted-F PCB antenna, which is commonly used for 2.4 GHz signals and is more cost-effective than antenna chips. To have this antenna work properly, a four-layer PCB design is necessary to provide the required thickness of individual PCB layers, which is critical for impedance match for the RF front end.

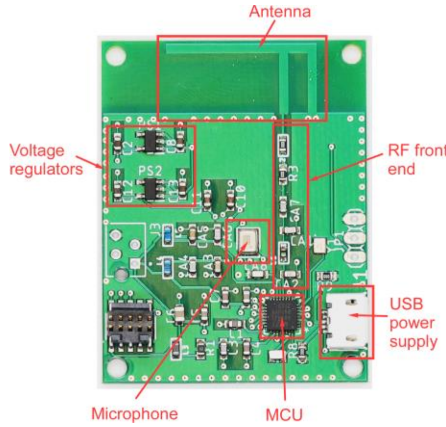


**Fig. 17.** Fabricated Main PCB.

For the SM2, the temperature sensors are placed on a separate SM2 plug-in PCB (Fig. 18) to maintain better thermal isolation from the main PCB. It also allows easier integration of the SM2 PCB on the waterpipe so that it can make direct contact with the waterpipe for thermal coupling. A cable with a 4-wire connector connects the main PCB to the SM2 plugin PCB.

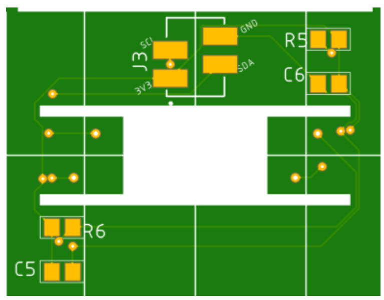


**Fig. 18.** SM2 Plug-in PCB Design.

The main PCB has undergone multiple revisions. Table 2 summarizes the key features of the revisions. The initial version, V1, incorporated sensor functions with wireless communication capability. In the V2 version, the analog microphone was replaced with the digital microphone to address the sensitivity issue of the analog microphone. The V3 version was designed to optimize the RF front-end design for enhanced wireless performance.

**Table 2.** Comparison Table of Main PCB Revisions.

| Version # | Key feature | SM1 Sensor | Board size (L×W [mm]) |
|---|---|---|---|
| **V1** | Initial design | Analog microphone | 44.49 ×35.61 |
| **V2** | Replace the analog microphone with a digital one. | Digital microphone | 45.97×35.56 |
| **V3** | Optimize RF front end with enhanced wireless performance | Digital microphone | 45.97×33.02 |

### 3.2.7. Power Budget and Lifetime Estimation for Sensor Module

Table 3 shows the power budget and lifetime estimation for the sensor module. The MCU will remain on all the time, either in the active or wireless transmitting mode, and the microphone will be woken up by the MCU every 0.5 s to monitor the water flow sound and perform detection. The sensor module is powered by a high-capacity, compact battery of 10 000 mAh. The sensor module is estimated to operate with a lifetime of at least 51 days under the assumptions including 50 measurements (or water flow events) per day, average duration of water flow events of 30 s, usable battery capacity at 80% of rated capacity, and others related to MCU energy modes. The battery can be replaced with a different size or capacity; if required, two or more batteries can be used together to provide an even longer lifetime.

**Table 3.** Power Budget and Lifetime Estimation of The Battery-Powered Sensor Module.

| Components | MCU | T Sensors x 2 | Heating Element | Microphone | Regulator | MOSFET Resistor (1 KΩ) |
|---|---|---|---|---|---|---|
| **Duty Cycle % (Active)** | 99.76 | 1.38 | 1.38 | 1.39 | 100 | 1.38 |
| **Duty Cycle % (Standby)** | 0 | 98.61 | 98.61 | 98.60 | 0 | 98.61 |
| **Duty Cycle % (Transmitting)** | 0.23 | - | - | - | - | - |
| **Average Current (mA)** | 2.52 | 0.008 | 3.64 | 0.01 | 0.21 | 0.04 |
| **Average Power (mW)** | 8.32 | 0.02 | 33.33 | 0.037 | 0.82 | 0.15 |
| **Total Energy/Day (J)** | 719.1 | 2.51 | 2880 | 3.22 | 71.56 | 13.06 |
| **Battery Capacity (mAh)** | 10 000 (assume 80% usable) | | | | | |
| **Battery Lifetime (days)** | ≈51.44 | | | | | |

### 3.2.8. Cost Estimation of Sensor Module for Volume Production

As the number of units increases toward larger volume production, the unit price of each sensor module unit drops considerably. Table 4 shows the estimated price breaks of the sensor module. The PCB component prices were obtained from Digikey and Mouser. Estimates of PCB fabrication and assembly costs were from PCBWay, a PCB manufacturing company. The package was 3D printed for the small quantity used for prototyping, while the cost can be significantly reduced for large quantities by using injection molding.

**Table 4.** Cost Estimation for Volume Production.

| Volume | 10 | 100 | 500 | 1000 |
|---|---|---|---|---|
| **MCU** | $6.76 | $5.53 | $4.61 | $4.61 |
| **Microphones** | $7.56 | $6.19 | $5.28 | $4.75 |
| **Connectors** | $1.16 | $0.96 | $0.85 | $0.70 |
| **Other PCB components** | $5.72 | $3.95 | $3.26 | $2.83 |
| **PCB components total** | $21.20 | $16.63 | $14.00 | $12.89 |
| **PCB fabrication** | $6.12 | $1.01 | $0.41 | $0.20 |
| **PCB assembly** | $11.29 | $5.96 | $2.18 | $1.33 |
| **Power bank (est.)** | $20.00 | $15.00 | $12.00 | $10.00 |
| **Other accessories** | $1.22 | $1.12 | $0.96 | $0.88 |
| **Packaging (est.)** | $10 | $8 | $5 | $3 |
| **Unit Cost Total** | **$69.83** | **$47.72** | **$34.55** | **$28.30** |

## 3.3. Sensor Network Implementation

### 3.3.1. Overview

The wireless network for the distributed sensor system will be based on the Zigbee protocol, which is a low-power and low-cost wireless communication standard developed based on the IEEE 802.15.4 technical standard. Compared to other low-power wireless technologies such as Bluetooth Low Energy (BLE), Zigbee can form a stable, reliable, scalable, and easily reconfigurable mesh network for battery-powered devices. Other advantages include a significantly larger limit on the number of nodes (up to a theoretical limit of 65 000), virtually unlimited range through data relaying, and wall penetration. The mesh network configuration also enables redundancy; data can be transmitted through an alternative route if any node fails due to a drained battery or other malfunction.

### 3.3.2. Zigbee Wireless Network Configuration

Zigbee Wireless network (Fig. 19) will have a central unit that will act as a gateway and allow internet connections through Wi-Fi. This will give the users remote access from a laptop or smartphone to the gateway to manage the sensor network and wirelessly collect the recorded sensor data through the Internet. The gateway will have 2 components. The first is a Raspberry Pi, a credit-card-sized computer with built-in Wi-Fi capability; the other is the microcontroller chip with a built-in Zigbee function to connect to sensor modules in the sensor network. For the implementation of the gateway, a circuit board with the microcontroller chip will be attached to the Raspberry Pi via the USB port. Each sensor module in the Zigbee network receives commands and settings from the gateway and reports sensor data to the gateway. A custom-defined data frame/structure will be used for the data report.

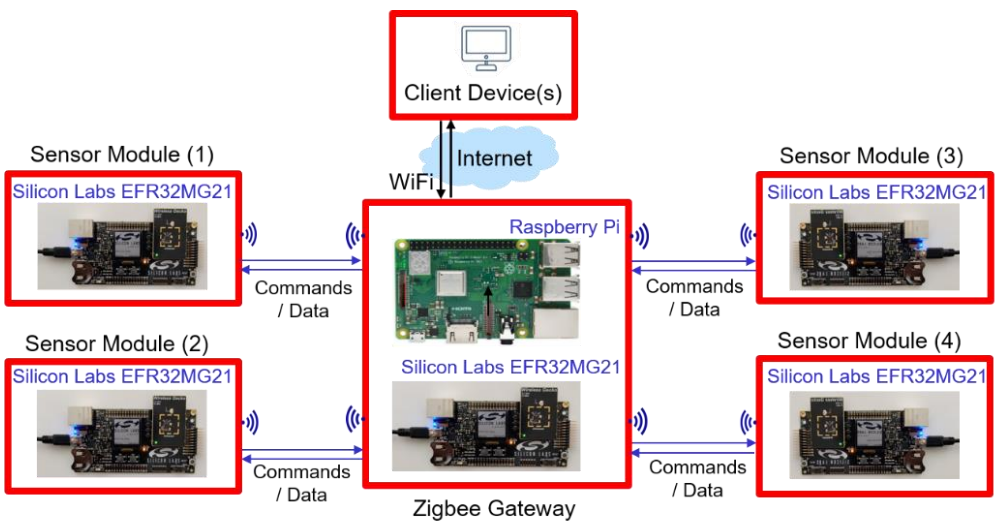


**Fig. 19.** Zigbee Network Topology.

### 3.3.3. System Software Architecture

The software for the entire system is organized into 3 logical blocks, which follow the network hierarchy, comprising of the sensor modules, the wireless network gateway (based on the selected Zigbee protocol), and the remote computer / end-user device (Fig. 20). At the lowest level we have the sensor modules, which will be installed at various water monitoring locations. The sensor module consists of multiple functional blocks, namely, SM1, SM2, Zigbee communications functions, data management and storage, and power management block. SM1 has an ADC operation and data processing block – to read and process the acoustic data from the microphone and a water flow detection algorithm based on the acoustic data. SM2 comprises of a heater control module - to control the on/off of the heater, a temperature sensor interface – to read thermal data from the temperature sensors, and a water flow detection algorithm based on the data.

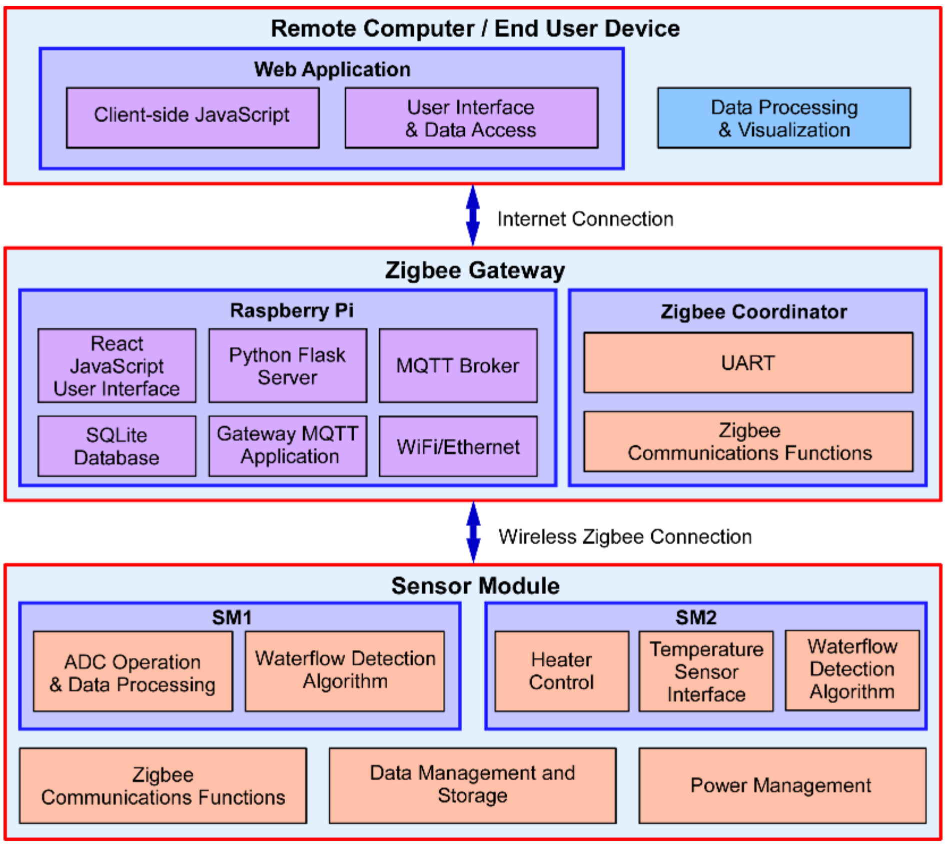


**Fig. 20.** System Software Architecture.

The sensor modules will be connected to the central unit wirelessly over Zigbee. We have the central unit in the middle, which acts as a gateway between the sensor modules and the internet. The gateway consists of a Raspberry Pi and a Zigbee coordinator. The Zigbee coordinator, which uses the same MCU as the sensor modules, has a Zigbee communication functions block – to communicate with the sensor modules wirelessly and a UART interface – to communicate with the Raspberry Pi. The Raspberry Pi has various blocks for serving the user interface webpage and interfaces the Zigbee network with the Internet through Wi-Fi or Ethernet connection. Finally, at the top, we have the remote computer where the end user will access the developed user interface through a web browser where the client-side Javascript will run. Further data processing and visualization can be achieved by operating native applications remotely.

### 3.3.4. Data Frame Definition

Figure 21 illustrates the definition of the data that will be wirelessly transmitted from the sensor module to the Zigbee gateway. First, we have the Zigbee header, which is intrinsic Zigbee data that is necessary to start the data frame. Following the Zigbee header is the user data. The user data will include the results from both sensor modalities, including SM1 and SM2, where SM1 is acoustic, and SM2 is thermal. This includes the start and stop time stamps of the water flow event detected by SM1 (A and B). Next, we have the start and stop time stamps detected by SM2 (C and D). After that, we have the temperature of the pipe and the temperature difference measured within the thermal flow sensor. Finally, we have an optional field for flow rate, which can be generated based on the results from SM1 or SM2.

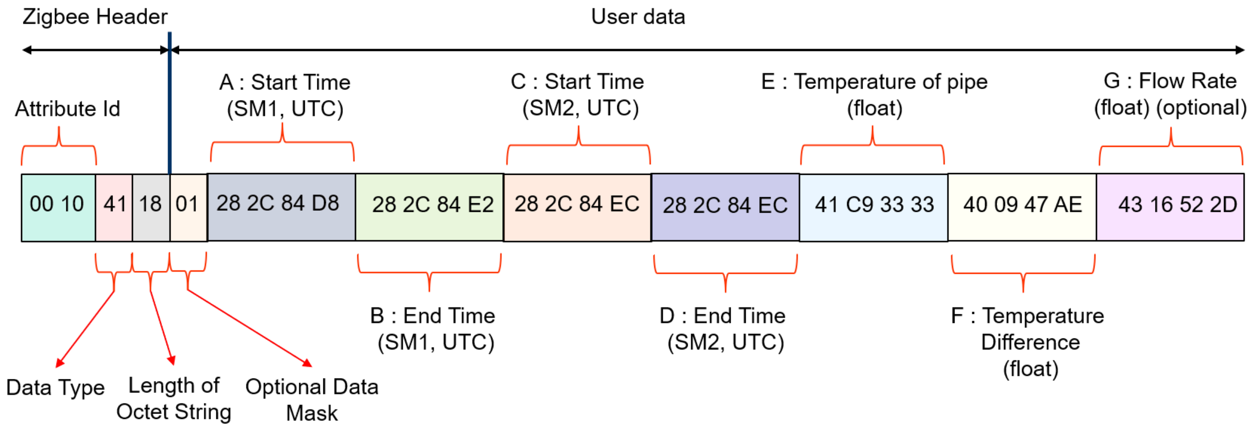


**Fig. 21.** Custom Data Frame Used to Report Data from End Device to Gateway.

### 3.3.5. Web-Based Remote User Interface

Figure 22 shows the developed remote user interface as a web application that the user can remotely access from a web browser to manage the sensor modules and sensor network and retrieve the data. Figure 22 (top) shows the screenshot of the web application that lists connected sensor modules in the sensor network. As an example, shown in the figure, two units were listed with their IDs, the locations of the sensors, and other information. Figure 22 (bottom) shows the event data collected wirelessly over the Zigbee network from each sensor module.

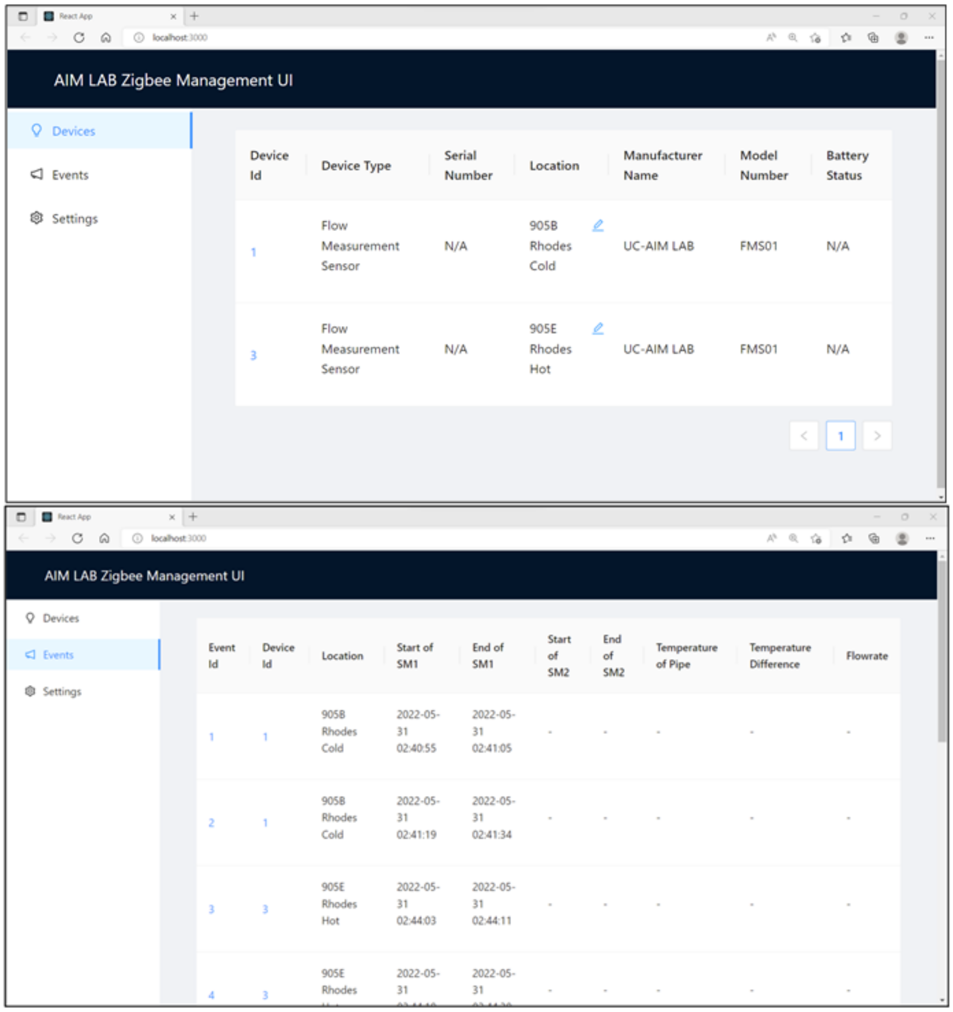


**Fig. 22.** Web-Based Remote User Interface.

## 3.4. Experimental Evaluations of Sensor Module and Sensor Network

### 3.4.1. Sensor Modality 1 Testing

We performed benchtop tests of the selected algorithm for SM1 on its capability to detect the water on/off events while some noises are in the background. These tests included 6 different audio recordings, each with the water flow sound mixed with different noises (either one type of noise or a combination of different noises). These tests used an audio recording of water flow sound mixed with noises in a single audio file. The water flow signal had a flow rate of 1.05 GPM , and noise signals had a typical sound level.

Table 5 shows the different audio files used in these tests with various types of noise mixed in the water flow sound and the test results. The algorithm successfully processed all audio recordings to detect correct on/off events. The algorithm was then tested in Stage-1 field tests to evaluate its performance in actual conditions, and details are reported in Sec. 3.4.3.

**Table 5.** Different Audio Recordings and Their Test Results.

| Recording | Noises | Water flow duration (sec) | Detection successful? |
|---|---|---|---|
| **#1** | Doctor office | 3-8 | Yes |
| **#2** | Music (soft beats) | 3-8 | Yes |
| **#3** | Hospital hallway | 3-8 | Yes |
| **#4** | Reception desk + Hospital hallway | 1-6 | Yes |
| **#5** | Patient room | 2-7 | Yes |
| **#6** | Patient room + music | 2-7 | Yes |

### 3.4.2. Sensor Modality 2 Testing

#### 3.4.2.1. SM2 Test Setup

To facilitate the test of the SM2 thermal detection approach on water pipes of different materials and sizes, we developed a test setup that is compact to fit on the lab bench and easy to control water flow during the tests. The schematic diagram (Fig. 23 left) shows the design of the test setup, including both PEX pipes and copper pipes, each with sizes of 1/4”, 3/8”, 1/2”, and 3/4”. Two manifolds, one upstream and one downstream, are used to assemble all test pipes. Valves are included on each test pipe to allow individual water flow control. The test setup is connected to the water faucet in the lab through a digital inline flow meter that is used to monitor the flow rate and provide reference data for calibrating the optional flow rate measurement function of the SM2 sensor modality. Figure 23 (right) shows a photo of the test setup. Compression fittings are used at all joints to allow reconfiguration of the test setup if it becomes necessary. The test setup is assembled on a wood board and raised for operation convenience around the pipes using wood studs.

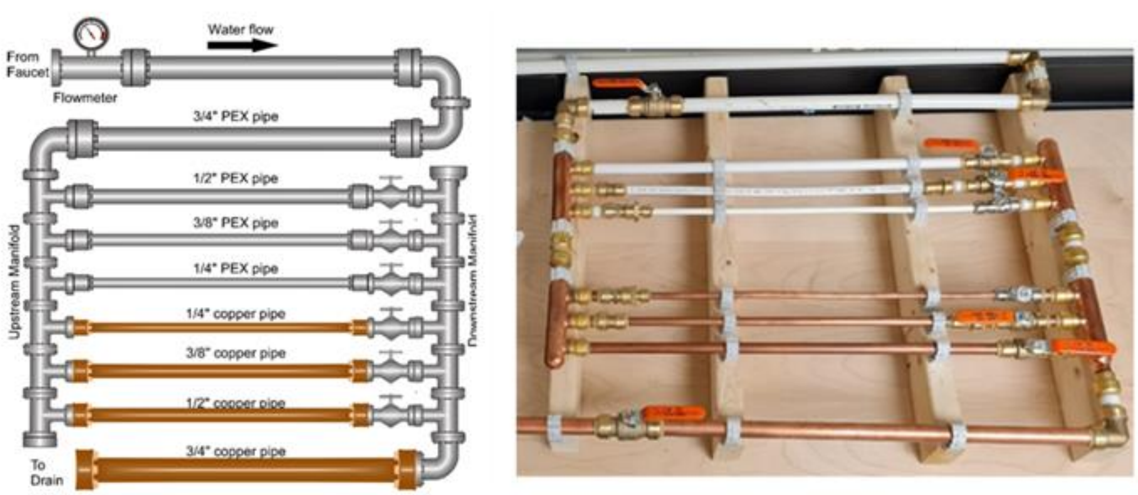


**Fig. 23.** Schematic of Test Setup Design (left) and Photo of Implemented Setup (right).

### 3.4.2.2. Experimental Results for “L” Optimization

A series of experiments were performed to optimize the distance of L using the setup shown in Fig. 24 that allows L to be varied. The results from the experiment are plotted in Fig. 10, shown as orange dots. The test results indicate an optimal L of ≈12 mm, which is consistent with the simulation results shown as blue dots.

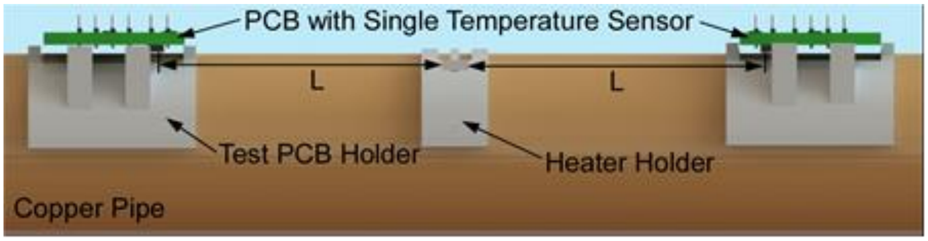


**Fig. 24.** Distance Optimization Test Setup.

### 3.4.2.3. Experiment to Evaluate Heat Conduction Symmetry

The symmetry of heat conduction from the heater is important to minimize sensor offset. This was experimentally evaluated with the assembled device mounted on a copper pipe, as shown in Fig. 24. The heater was turned on with a pipe filled with (nonflowing) water. The recorded readings from both T1 and T2 temperature sensors are plotted in Fig. 25. Both T1 and T2 readings here showed a consistent increase of ≈1°C after the heater was turned on. The ΔT shown in brown color remained stable within a small range of ≈0.05°C, indicating excellent symmetry of heat conduction from the heater achieved by the symmetric design of device structure and thermal insulation.

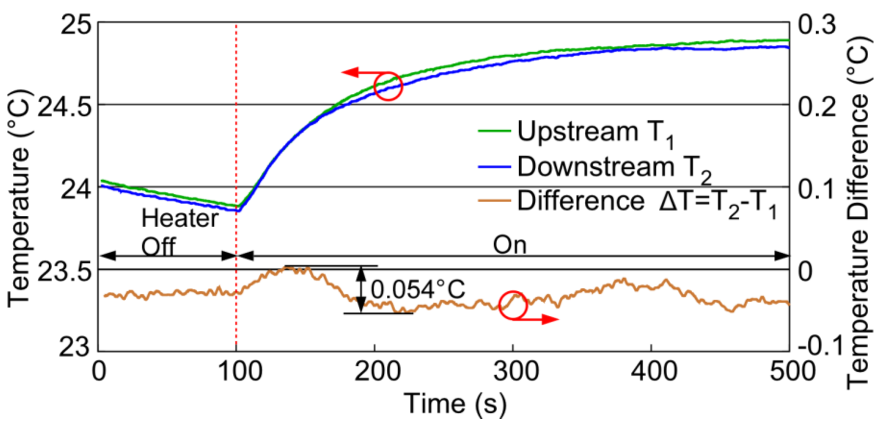


**Fig. 25.** Experimental Results Showing T1 and T2 Readings and ΔT from a Single Flow Event.

### 3.4.2.4. Experiments with Repetitive Waterflow On/Off Events

The assembled device was deployed for waterflow event detection to evaluate its effectiveness using the setup shown in Fig. 24. The heater was turned on and the waterflow was turned on and off to emulate water usage events at a fixture. Figure 26 shows the recorded T1 and T2 temperature readings in blue and green curves and calculated ΔT in the brown curve. These curves show a clear pattern following the water on/off cycles, successfully verifying the principle and functions of the calorimetric sensor and indicating that the device operates effectively. A small delay of 0 s to 3 s was observed and is not expected to affect the target application.

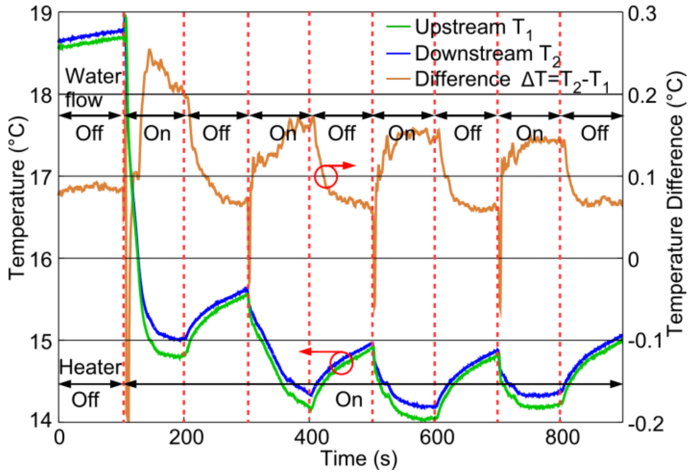


**Fig. 26.** Experimental Results Showing T1 and T2 Readings and ΔT from Multiple Flow Events.

### 3.4.3. Stage-1 Field Testing

We performed Stage-1 field tests using the setup and configurations shown in Sec. 3.2.5. Initial Stage-1 field tests were performed using the analog microphone, which was later changed to a digital microphone due to the consistency issue with the analog microphone.

#### 3.4.3.1. Stage-1 Field Tests Using Analog Microphone: Initial Results and Issues

In the initial Stage-1 field test performed in March 2022 in the restrooms of the Marian Spencer Residence Hall of the University of Cincinnati, two sensor modules, both using an analog microphone, were used to record 5 seconds of sound data every 15 s; each module was deployed on the waterpipe connected to faucets in either the men's or women's restroom. The recorded sound data were stored on the Raspberry Pi for post-processing. Automation scripts were developed to process the recordings and select those with significant sound levels for further processing. A manual review of about 3000 recordings was also done for this test to confirm the accuracy of the automation scripts. We identified 9 out of the 4163 recordings for men's and 310 out of 4240 for women's restrooms related to water flow.

We performed the 2nd test soon after the initial test to revalidate the results, but somehow the device lost the capability to record the water flow sound properly, and it could not detect any water use events. Since then, we have performed a series of field tests to diagnose the issue using various approaches both in our lab and in the field to try to identify the cause of the issue. We compared alternative microphones such as a commercial ECM or electret condenser microphone, a type of small cylinder shape microphone that can be worn on clothes and has high sensitivity, along with other microphone chips that can be integrated with the PCB. Using these alternative microphones during the 5th and 6th field tests, we could detect the water use events again. Fresh analog microphone chips were also tested but gave the same results as those on our test devices, indicating it was not due to degradation of the analog microphone chip.

Due to the issue with the analog microphone, we evaluated alternative microphone chips that can still be integrated with PCB and have a similar footprint but without the wakeup function of the analog microphone chip. These chips have a digital interface that is much more popular and widely available in the market. We chose a Knowles digital microphone as an alternative because it has better sensitivity than others.

#### 3.4.3.2. Stage-1 Field Tests with New Digital Microphone

Figure 27 shows the photo of the deployed system with the new digital Knowles microphone for Stage-1 testing. The digital microphone is connected to the Raspberry Pi unit over the $I^2S$ interface. The Raspberry Pi is powered by a 5 V rechargeable lithium-ion battery pack. The microphone is mounted on the waterpipe using the coupling ring.

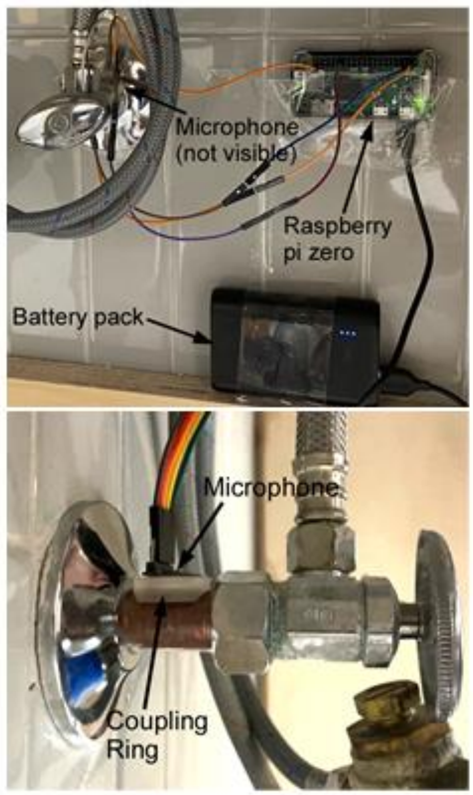


**Fig. 27.** Stage 1 Deployed System with New Digital Microphone.

#### 3.4.3.3. Reference Sensor

A reference sensor (Fig. 28) was required to validate and crosscheck our deployed system's detected water flow events. Initially, we used an ultrasonic reference flow sensor by Keyence at the test site during the 2nd and 3rd field test to measure the flow rate when there was water usage. The Keyence flow sensor could record flow rate; however, it did not meet the needs for reference detection as it could only record flow rate at a maximum frequency of one data point every 10 sec due to limitations in memory and its need for stabilization of ultrasound signal. We then used the TDS-100H flow meter, which is also based on an ultrasonic mechanism but allows the user to record data at a frequency as high as 1 Hz (once every second). It has a built-in rechargeable battery that lasts about 10 hours and can be extended using an external battery source.

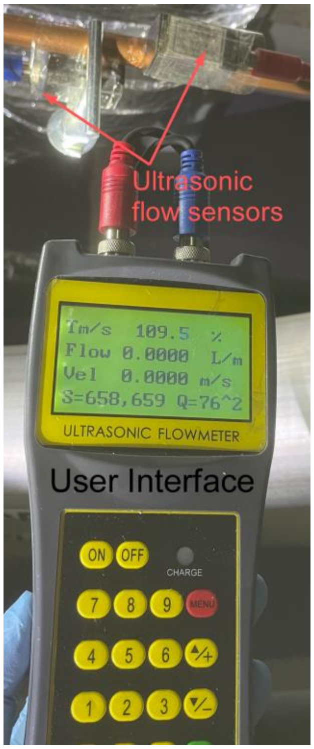


**Fig. 28.** TDS-100H Ultrasonic Flowmeter.

#### 3.4.3.4. Summary of Stage-1 Field Tests and Example Results

Table 6 summarizes all the stage-1 field tests done to date. Starting in field test #12, an ultrasonic reference sensor was deployed along with the digital microphone for calibration and crosscheck of the sensor. The reference sensor proved helpful in identifying the false triggering from the periodic interference and further enhancing the detection algorithm.

**Table 6.** Summary of Stage-1 Field Tests.

| Stage-1 test # | Test duration (Start date) | Location | No. of sensors deployed | Additional information | Proper event detection |
|---|---|---|---|---|---|
| **1** | 24 hrs. (3/15/2022) | Marian Spencer Hall | 2 (Men's & Women's restrooms) | No insulation or reference flow sensor | Yes (PUI Audio mic.) |
| **2** | 24 hrs. (4/12/2022) | Marian Spencer Hall | 2 (Men's & Women's restrooms) | One sensor insulated; reference flow sensor used | No (PUI Audio mic.) |
| **3** | 24 hrs. (4/21/2022) | Marian Spencer Hall | 2 (Men's & Women's restrooms) | Different coupling rings tested; reference flow sensor used | No (PUI Audio mic.) |
| **4** | 4 hrs. (5/6/2022) | Marian Spencer Hall | 2 (Men's & Women's restrooms) | Different coupling rings tested | No (PUI Audio mic.) |

| Stage-1 test # | Test duration (Start date) | Location | No. of sensors deployed | Additional information | Proper event detection |
|---|---|---|---|---|---|
| **5** | 4 hrs. (5/12/2022) | Marian Spencer Hall | 1 (Men's restroom) | Also tested commercial ECM | Yes (ECM) |
| **6** | 4 hrs. (5/26/2022) | Marian Spencer Hall | 1 (Men's restroom) | Also tested ECM & other microphone chips | Yes (ECM & alt. mic.) |
| **7** | 27 hrs. (8/9/2022) | Rhodes 939 | 2 (Men's restroom on 2 faucets) | 3 hr. data for one sensor (memory full) | Yes (Knowles SPH0645) |
| **8** | 44 hrs. (8/14/2022) | Rhodes 939 | 2 (Men's restroom on 2 faucets) | 3 hr. data for one sensor (memory full) | Yes (Knowles SPH0645) |
| **9** | 22 hrs. (8/16/2022) | Marian Spencer Hall | 2 (Men's & Women's restrooms) | Periodic interference observed. | Yes (Knowles SPH0645) |
| **10** | 24 hrs. (8/17/2022) | Marian Spencer Hall | 2 (Men's & Women's restrooms) | Periodic interference observed. | Yes (Knowles SPH0645) |
| **11** | 23 hrs. (8/18/2022) | Marian Spencer Hall | 2 (Men's & Women's restrooms) | Periodic interference observed. | Yes (Knowles SPH0645) |
| **12** | 10.25 hrs. (8/19/2022) | Marian Spencer Hall | 1 (Men's restroom) | Periodic interference observed; ultrasonic reference sensor used | Yes (Knowles SPH0645) |
| **13** | 22 hrs. (8/23/2022) | Marian Spencer Hall | 2 (Men's restroom) | Ultrasonic reference sensor mounted in men's restroom | Yes (Knowles SPH0645) |
| **14** | 44 hrs. (09/13/2022) | Marian Spencer Hall | 2 (Men's restroom) | Ultrasonic reference sensor mounted in men's restroom | Yes (Knowles SPH0645) |
| **15** | 48 hrs. (09/27/2022) | Marian Spencer Hall | 2 (Men's restroom) | Ultrasonic reference sensor mounted in men's restroom | Yes (Knowles SPH0645) |
| **16** | 23 hrs. (09/29/2022) | Marian Spencer Hall | 2 (Men's restroom) | Ultrasonic reference sensor mounted in men's restroom | Yes (Knowles SPH0645) |
| **17** | 96 hrs. (10/03/2022) | Marian Spencer Hall | 2 (Men's restroom) | Ultrasonic reference sensor mounted in men's restroom | Yes (Knowles SPH0645) |

For example, the results of Stage-1 field test #17, a test of 96 hours, are shown in Figs. 29 and 30. In this test, the reference sensor recorded data only during the day as it can store only a maximum of 18 hours of data, and long duration is necessary to transfer the stored data to a computer. Figure 29 shows a distribution of the number of events recorded every day during the test. The lighter blue bars in this plot show the number of events detected by our sensor, whereas the orange ones are from the reference sensor, and the darker blue shows the number of events by our sensor when both the sensor and reference are working. The Figure shows that events recorded by our SM1 sensors closely match the reference sensor. Figure 30 shows a distribution of recorded events based on the duration of the events.

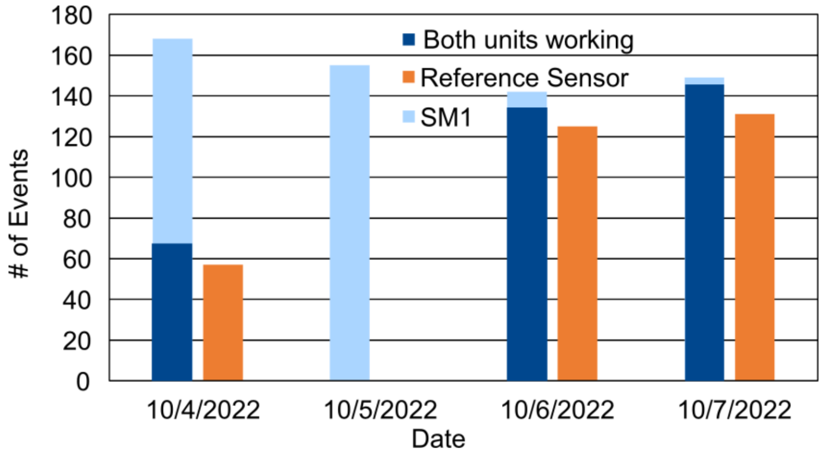


**Fig. 29.** Waterflow Events Recorded in the Men's Restroom During Field Test #17.

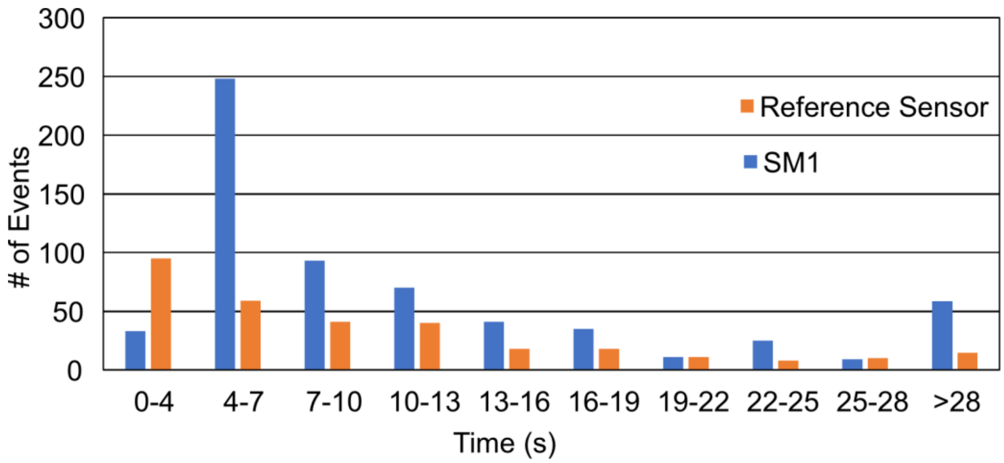


**Fig. 30.** Distribution of Recorded Event Duration.

### 3.4.4. Field Test of Complete Sensor Module

With successful Stage-1 field tests and an improved algorithm, we performed additional field tests using integrated sensor modules with an algorithm embedded in the MCU for in-situ real-time detection of water flow events. The entire water flow detection algorithm was ported from Matlab to the MCU, with optimization to account for the computing power differences between the regular computer and the ARM core microprocessor inside the small MCU chip.

The ported algorithm and the main PCB were tested in the other field test site at the men's restroom in Rhodes 939 at the University of Cincinnati. The setup for the field test is shown in Fig. 31. The main PCB with the sensor was mounted on the flex hose for the faucet as the copper pipe exposed outside the wall was too short to mount the PCB. The software was configured to perform data processing on the MCU and then output the calculated signal strength indicator (SSI) values to the computer for verification of the algorithm functionality. A series of water flow events of varying durations were manually performed on the faucet to test the detection capability of the sensor and algorithm. Figure 32 shows a plot of the collected SSI values versus time, showing the clean and accurate results of the water flow events, and confirming the successful porting of the algorithm to MCU.

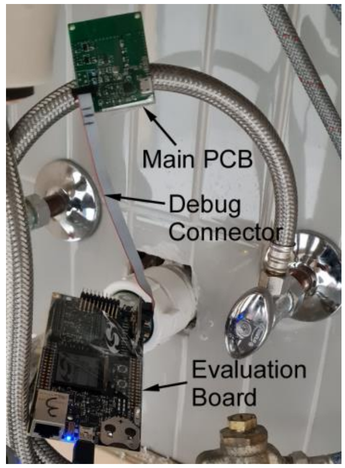


**Fig. 31.** Test Setup.

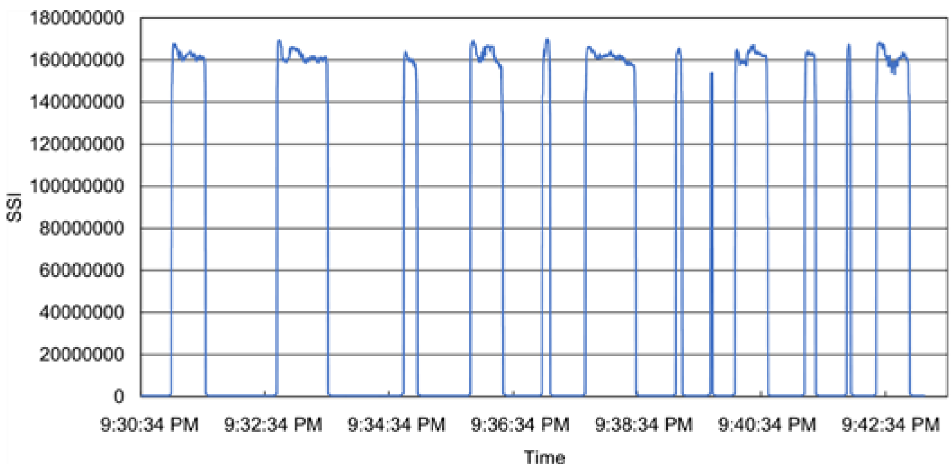


**Fig. 32.** Recorded SSI Values.

### 3.4.5. Wireless Sensor Network Evaluation

#### 3.4.5.1. Wireless Performance Test

We performed tests on the fabricated main PCB to verify the quality of Zigbee wireless communication by sending one thousand data packets between the main PCB and the Zigbee coordinator and monitoring the packet error rate (PER). Figure 33 shows the test setup. The main PCB was connected to a SiLab evaluation board, which was then connected to a computer to monitor the data transfer. The antennas on the Zigbee coordinator and the main PCB pointed at each other for the best signal transmission. The main PCB was placed 1.2 m away from the Zigbee coordinator to simulate the physical separation when deployed. Both the transmitting and receiving performances of the main PCB were tested. For comparison, a reference test was performed between two commercial PCBs with the standard implementation of the Zigbee RF front end. The test results indicated that the main PCB had a 0.1% higher PER than the reference test when transmitting and 0.5% higher when receiving. This is within a reasonable range and can be accommodated by the self-correction function of the Zigbee protocol and, therefore, will not affect the Zigbee communication.

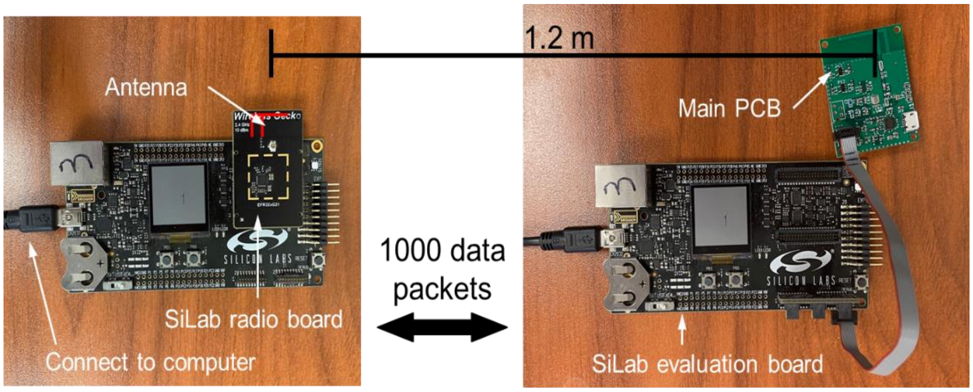


**Fig. 33.** Setup of Wireless Performance Test.

#### 3.4.5.2. Overall System Deployment Test

Overall system deployment tests, including multiple sensor modules with SM1 and SM2 functions and the Zigbee wireless communication over the sensor network, were performed.

Figure 34 shows an approximate layout of the testing site. The Zigbee gateway was deployed at one corner of room 905B Rhodes, while two sensor modules were mounted on ½” copper pipes nearby regular water faucets in either Test Site 1 or 2 in separate rooms. The distances between the sensor modules and the Zigbee gateway were 3 m and 18 m, respectively.

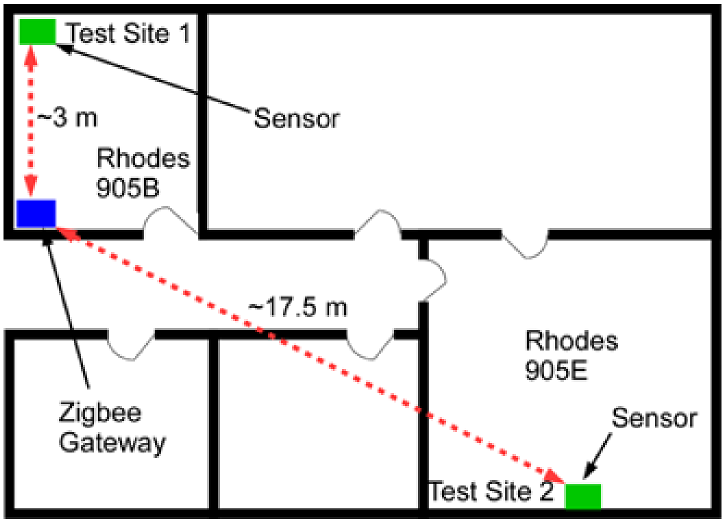


**Fig. 34.** Approximate Layout of a Testing Site.

Both sensing modalities in the sensor module were tested concurrently for water flow detection. The data were wirelessly recorded into the Zigbee gateway and downloaded through the user interface on the web application. A subset of the recorded water flow events with timestamps is listed as examples in Table 7. A delay of 0 s to 3 s was observed between the event timestamps generated by SM1 and SM2, which is as expected and considered acceptable. The wireless sensor network system was successfully verified for its operation and functions for the intended application.

**Table 7.** Recorded Water Flow Events with Timestamps.

| Events | Location | SM1 Timestamps (sec) | | SM2 Timestamps Raw data (sec) | |
|---|---|---|---|---|---|
| | | On | Off | On | Off |
| **1** | 1 | 0 | 103 | 1 | 103 |
| **2** | 1 | 200 | 303 | 202 | 303 |
| **3** | 1 | 400 | 502 | 401 | 503 |
| **4** | 1 | 600 | 702 | 603 | 702 |
| **5** | 1 | 800 | 903 | 802 | 903 |
| **6** | 1 | 1000 | 1103 | 1003 | 1103 |
| **7** | 1 | 1200 | 1303 | 1201 | 1303 |

In summary, Task 1 successfully developed and beta tested of low cost, battery-powered, miniature wireless sensor module for non-invasive detection of water flow through pipes in a building. When deployed in a typical premise plumbing pipe network, the modules form a wireless sensor network that accurately monitors and continuously records the incidence and patterns of water usage at various select fixtures. These readings can be analyzed to infer the frequency or probability of fixture use, as described in the following section of this report.

## 4. Task 2: Data Analysis

This section presents statistical analysis of the data collected using the wireless sensor network, the methods of calculating fixture probability of use, and examples of applying and validating the fixture *p*-values.

### 4.1. Exploratory Data Analysis

The wireless sensor network described in Section 3 was deployed at the recently constructed Marian Spencer Hall (MSH) located on the University of Cincinnati main campus. MSH is a 112,600 square feet mixed-use building with a cafeteria on the 1st floor, office space on the 2nd floor, and residential space with about 338 beds on the 3rd to 8th floors. The student spaces are suite-style, with four-bed spaces sharing a bathroom. The cafeteria has open seating with various service locations catering to baked foods, deli, grilled foods, and desserts. Lunch and dinner are served every day between 10:30 am and 8:00 pm during the fall and spring semesters and only lunch on weekdays during the summer semester.

Sensors were installed on a ½ inch domestic cold water supply pipe connected to two lavatory sinks in the men’s and women’s restroom at the MSH cafeteria. Figure 35 is a schematic diagram of the supply pipes to the sink fixtures in the cafeteria restroom.

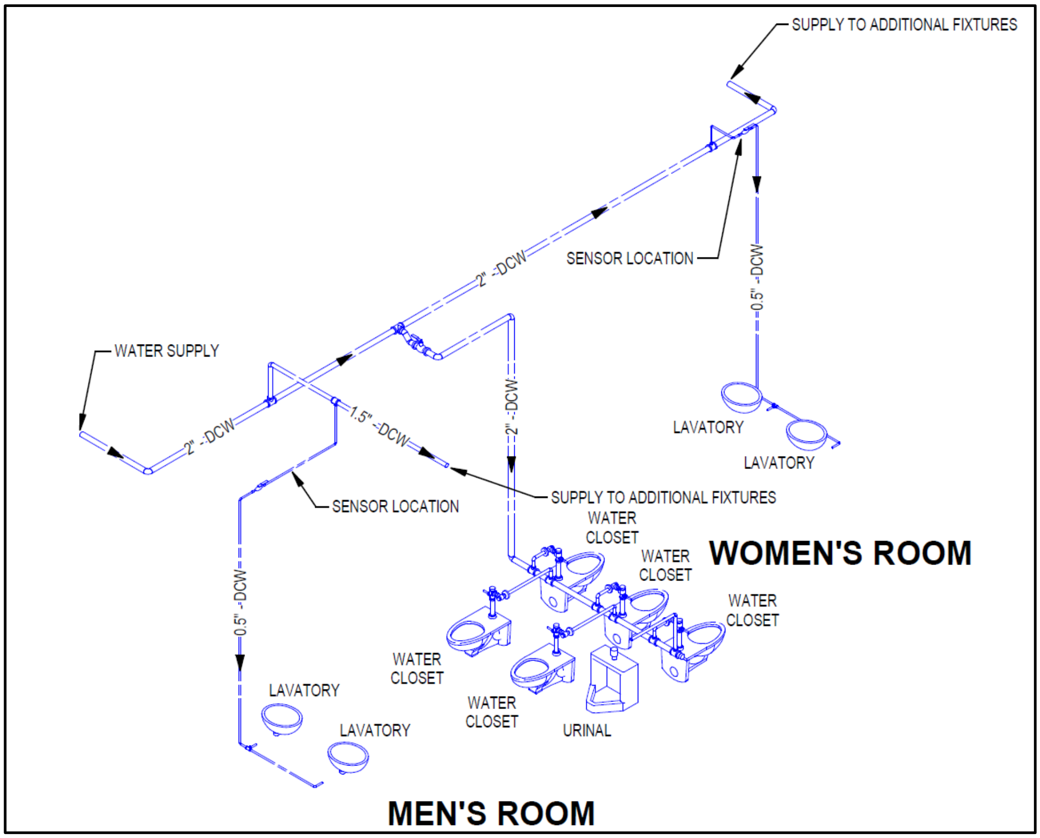


**Fig. 35.** Plumbing Layout at the MSH Cafeteria Restroom Indicating Sensor Locations (not drawn to scale)

Pilot tests were conducted for the wireless sensor network in the cafeteria restroom of the MSH building. Water use data indicating start and stop times for lavatory use were logged over 24 hours on non-consecutive days during the summer and fall semester 2022. Table 8 summarizes daily flow statistics for lavatories in the men's and women's restrooms.

**Table 8.** Average Daily Statistics of Water Use from Two Lavatories at the Men's and Women's Restrooms in the MSH Cafeteria.

| Daily Statistics | Men's Restroom (23 days) | | Women's Restroom (2 days) | |
|---|---|---|---|---|
| | Average | Range | Average | Range |
| **Number of logged events** | 152 | 81 - 205 | 71 | 62 - 80 |
| **Mean duration (seconds)** | 23 | 12 - 47 | 77 | 72 - 82 |
| **Standard deviation (seconds)** | 36 | 11 - 126 | 140 | 140 - 141 |
| **Minimum duration (seconds)** | 4.6 | 1.0 - 8.0 | 3.5 | 3.0 - 4.0 |
| **Maximum duration (seconds)** | 310 | 54 - 999 | 692 | 578 - 806 |

There are some notable differences in the daily characteristics of lavatory use in the men's and women's restrooms. Average daily events (fixture use) were higher in the men's restroom (152 per day) compared to the women's restroom (71 per day). However, the average daily duration of hand washing at the lavatories was longer in the women's restroom (77 seconds per use) than in the men's restroom (23 seconds per use). The probability of lavatory fixture use calculated from these data is discussed in Section 4.3, using methods described in Section 4.2.

## 4.2. Methods of Estimating Peak Period Probability of Fixture Use

A water fixture has two states. It is either busy (flowing water) or idle (not flowing water). The probability $p$ that a fixture is busy ("$p$-value") is a dimensionless quantity between 0 and 1 that represents the fraction of time the fixture is flowing water. This probability is found as a ratio of two time periods: total duration of fixture flow to total duration of fixture observation, as indicated in Eq (1),

$$p = \frac{\text{Total duration of fixture flow}}{\text{Total duration of fixture observation}} \tag{1}$$

Because indoor water use often follows a diurnal pattern, with alternating periods of high and low demand, the probability of fixture use varies during the day. Fixture $p$-values that occur during the daily peak period are relevant and necessary for design of premise plumbing systems. In this study, the peak period is taken as the hour during which the volume of indoor water consumption is greatest.

It is convenient to visualize water use at a busy fixture as a rectangular pulse with a constant rate of flow over some period of time. Figure 36 illustrates a sequence of $m$ rectangular water pulses observed at a single fixture.

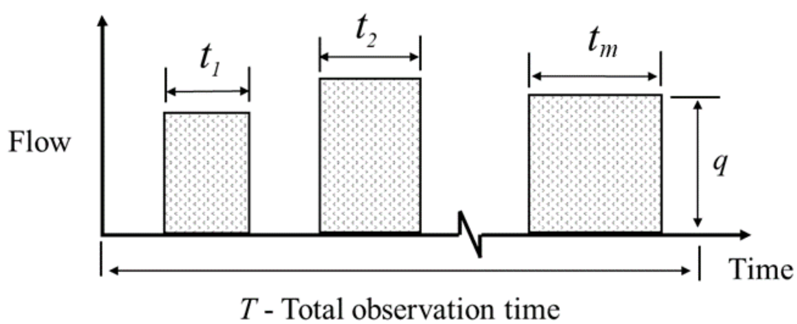


**Fig. 36.** Measured Pulses at a Fixture During the Observation Period.

Referring to Figure 36, the idea expressed in Eq (1) can be written,

$$p = \frac{\sum_{i=1}^{m} t_i}{T} = \frac{b}{T} \tag{2}$$

In Eq (2), $t_i$ is the duration of the $i^{\text{th}}$ use at the fixture, $m$ is the total number of water use events at the fixture during the peak period and $T$ is the duration of the observation window during the peak period (typically one hour). Comparing numerators in Eq (2) shows that $b$ is shorthand notation to represent the total time the fixture is busy during the observation period.

There are three basic methods to estimate the probability of fixture use given in Eq (2). They are:

- Monitor water use at individual fixtures and apply Eq (2).
- Observe steady-state customer arrivals and departures at fixture locations.
- Apply engineering judgment in conjunction with constraints imposed by a new ramp function on the dimensionless unit square.

All three methods are closely related to one another and are outlined in the following sections.

### 4.2.1. Method 1: Monitoring Water Use

Section 3 of this report described a sensor network capable of monitoring and recording the frequency and duration of water use at individual fixtures in a building. When high resolution fixture-level water use data are available, the probability of use for individual fixtures can be found from the ratio of two time periods as shown in Eq (2). This expression applies to data measured at a single fixture. If there are readings from $n$ multiple identical fixtures, Eq (2) becomes

$$p = \frac{\sum_{k=1}^{n} b_k}{\sum_{k=1}^{n} T_k} \tag{3}$$

Eq (3) provides a weighted average of the individual $p$-values computed from readings made at $n$ identical fixtures. The full duration of all busy time episodes at each of the $n$ identical fixtures is captured in the numerator. The full observation window of duration $T$ for each of the $n$ identical fixtures is reflected in the denominator. When $n$=1, Eq (3) simplifies to Eq (2).

The expression in Eq (3) was used by Omaghomi *et al.* [8] to estimate peak hour $p$-values from a large data set of high-resolution fixture level water use readings collected from over 1 000 residential households across the US. The resulting $p$-values for six household fixture groups (bathtub, clothes washer, dishwasher, faucet, shower, toilet) were used to calibrate the residential version of the Water Demand Calculator.

In principle, Eq (3) is simple to visualize; in practice, however, it is hard to apply. The main difficulty stems from a lack of high-resolution fixture level water use data needed to quantify the busy time values in the numerator of Eq (3). Monitoring water use at individual fixtures requires installation of special sensors throughout the premise plumbing system. This has been accomplished in a few instances for residential buildings (mainly single-family homes) where the fixture count is small.

Extending this approach to large commercial and industrial (CI) buildings faces daunting challenges because, in the CI sector, fixture types are more varied, fixture access is restricted and fixture counts tend to be much higher than in the residential sector. The sensor development work described in Section 3 of this report is a first step toward bridging this gap and providing a way to glimpse of the frequency and duration of water use at individual fixtures for buildings in the CI sector.

### 4.2.2. Method 2: Observing Arrivals and Departures

High resolution water use measurements at plumbing fixtures are very sparse. In lieu of in-situ measurements, observations of customer (pedestrian) traffic at fixture locations can lead to reasonable estimates of fixture use probability. This approach is best suited for "deterministic" fixtures, that is, ones where each use draws a set volume of water. To illustrate, consider the urinals in the men's restroom at large public facility like a sports arena, concert hall, convention center, international airport and so on.

Suppose the restroom has $n$ urinals which discharge a fixed volume of water $V$ at flowrate $q$ with each flush. Further, imagine "steady-state" operation where $N$ people enter and leave the restroom during an observation period of duration $T$. By "steady-state", it is meant that the overall rate at which people enter and leave the restroom is nearly the same and both rates are reasonably constant during the period of observation.

The ratio $V/q$ gives the duration of flow at a urinal during each flush. Assuming all $N$ people who enter the men's restroom use the urinal, the busy time term in the numerator of Eq (3) is

$$\sum_{k=1}^{n} b_k = \left(\frac{V}{q}\right) N \tag{4}$$

Similarly, with $n$ identical urinals, the observation time for the denominator of Eq (3) is

$$\sum_{k=1}^{n} T_k = nT \tag{5}$$

Putting Eqs (4) and (5) into Eq (3) and regrouping gives,

$$p = \left(\frac{N}{T}\right)\left(\frac{V}{q}\right)\left(\frac{1}{n}\right) \tag{6}$$

Equation (6) is an alternate version of Eq (3), expressed in terms that are relatively easy to monitor and measure in certain circumstances. During the period of observation, a line of people may form waiting to access the fixtures. The formation of a queue is known as congestion. Hunter [1] assumed congestion in his analysis of loads on plumbing systems because this condition is a worst-case scenario producing the highest demands on the building water supply.

To test Eq (6), water consumption was logged during 11 NCAA basketball games at the University of Cincinnati's Fifth Third Arena in early 2020 (data collection ended abruptly with the lockdown for the COVID pandemic). During halftime, the number of people exiting the men's and women's restrooms were monitored.

There were 48 restroom monitoring events at 15 different restroom locations (8 men, 7 women). With the pedestrian traffic data and knowledge of fixture operating characteristics, Eq (6) was used to calculate the $p$-value for the restroom fixtures (water closet, lavatory, and urinals). Figure 37 shows the flush valve $p$-value for the different men's and women's restrooms. On average, the flush valve $p$-values are 0.024 and 0.020 in the men's and women's restrooms, respectively.

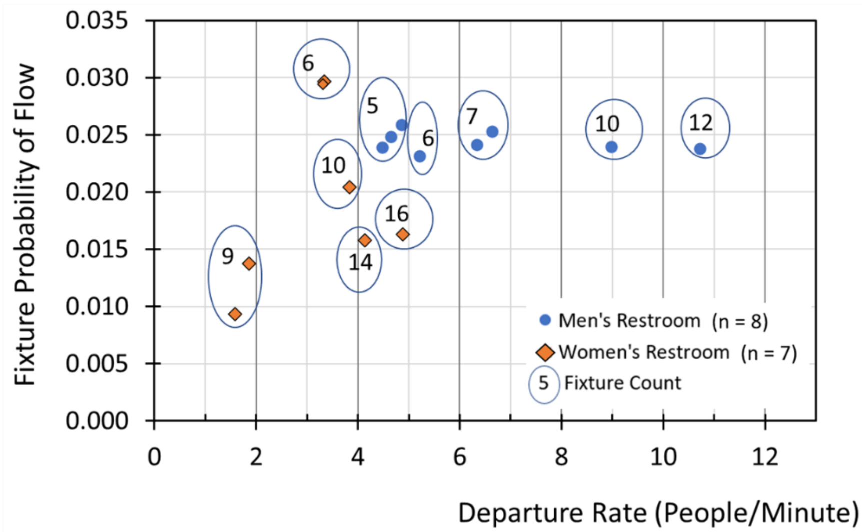


**Fig. 37.** Flush Valve *p*-values at The Fifth Third Arena.

Congestion from queue formation was common at the men's restroom (96 % of events) but rare at the women's restroom (15 % of events). The effect of pedestrian congestion at the men's restroom is evident in Figure 37 where fixture *p*-values plateau near 0.025 irrespective of the size of the restroom. As recognized by Hunter, congestion maximizes fixture *p*-values.

Taking average fixture *p*-values from Figure 37 and knowing the fixture types, the fixture counts ($n$) and the corresponding flowrates ($q$-values) for the court-accessible fixtures, the 99$^{th}$ percentile of the water demand during halftime at the Fifth Third Arena was calculated using the Wistort method,

$$Q_{0.99} = \sum_{k=1}^{K} n_k p_k q_k + (2.33)\sqrt{\sum_{k=1}^{K} n_k p_k (1 - p_k) q_k^2}$$

Figure 38 compares the peak flow predicted by Wistort's method in the Water Demand Calculator against the measured flow during the 20-minute halftime window on five men's game days. The predicted peak flow (dashed red line) is comparable to the 99$^{th}$ percentile (grey bar) and the maximum measured flow (blue bar) observed during half time.

The measured flows were logged at 3-s intervals with in-line meters on the cold water supply to the Fifth Third Arena. The good agreement between prediction and measurement in this example shows that use of Eq (6) with direct observation of pedestrian traffic offers a promising method for estimating realistic fixture *p*-values when in-line measurement of individual fixture use is not available.

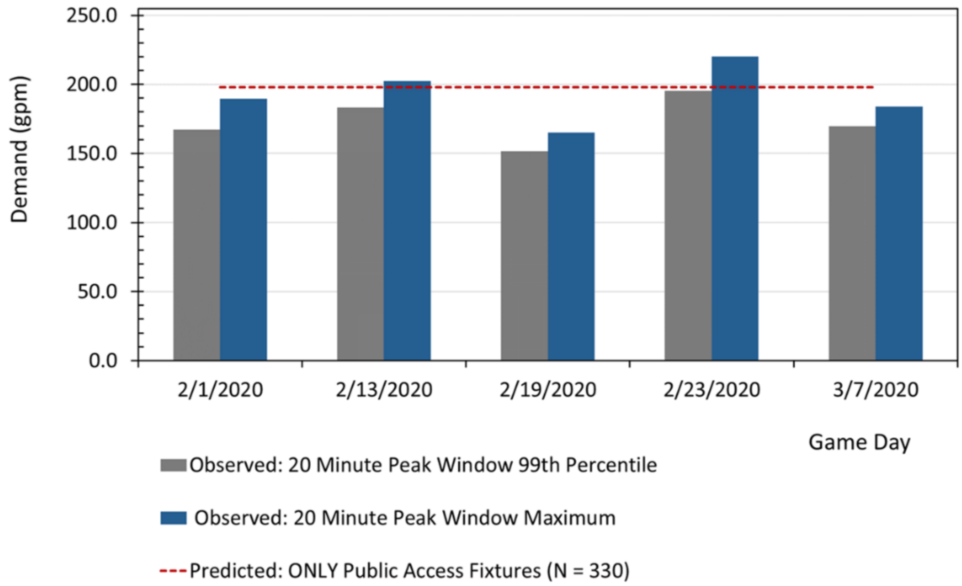


**Fig. 38.** Predicted Peak Flow using the WDC Compared to Measured Peak Flow in the Fifth Third Arena at the University of Cincinnati campus.

### 4.2.3. Method 3: Ramp Function on Unit Square

The lead term ($N/T$) in Eq (6) represents a steady-state rate of arrival or departure. At first glance, the structure of Eq (6) suggests that the computed fixture $p$-value increases with the magnitude of ($N/T$). This behavior is evident in the left-hand region of Figure 37, where the general trend of computed $p$-values grows with an increase in departure rate. In the right-hand region of Figure 37, however, the fixture $p$-values are constrained. The constellation of blue dots for the men's restroom hits a ceiling near a fixture $p$-value of 0.025.

The $p$-value plateau is the hallmark of congestion (queue formation). Congestion was common at the men's restrooms during halftime. Introducing a dimensionless ramp function on the unit square, it is possible to embed incipient congestion into Eq (6) and capture the plateau response seen in Figure 37. More importantly, this development offers a novel approach for generating preliminary estimates of fixture $p$-values in the absence of field data.

To begin, let $\lambda = N/T$ denote the steady-state rate of arrival or departure at a group of $n$ identical plumbing fixtures. Further, let $\tau = V/q$ denote the busy time during a single operation of a fixture; in other words, $\tau$ is the pulse duration. Then Eq (6) becomes

$$p = \frac{\lambda \tau}{n} \tag{7}$$

This expression can be viewed as an "unconstrained" estimate of the fixture $p$-value. Eq (7) is unconstrained in the sense that the computed $p$-value grows with an increase in the arrival rate, $\lambda$.

To impose a constraint on Eq (7), it is necessary to distinguish between two important time intervals at the fixture: (i) **busy time** (when water is flowing at the fixture) and (ii) **occupancy time** (when the presence or action of a user prevents others from using the fixture). For instance, consider a urinal in the men's restroom. The busy time for flowing water may last just a few seconds, but the duration of the occupancy time may approach a few minutes. Busy time cannot exceed occupancy time.

Let $T_O$ denote the average occupancy time at a fixture. During an observation window of duration $T$, the maximum number of arrivals that can be accommodated or serviced at a group of $n$ identical fixtures is given by $N_{MAX} = n[T/T_O]$. Substituting this term for $N$ in Eq (6) and simplifying gives

$$P_C = \left(\frac{n[T/T_O]}{T}\right)\left(\frac{V}{q}\right)\left(\frac{1}{n}\right) = \frac{\tau}{T_O} = \mu\tau \qquad (8)$$

Eq (8) represents the probability of fixture use at incipient congestion, designated here as $P_C$. It is the maximum $p$-value that can be attained at the fixture. It provides an upper bound on the results from Eq (7). In Eq (8), $\mu = 1/T_O$. This term is the inverse of the occupancy time and is known as the service rate of the individual fixture. Combining Eqs (7) and (8) leads to

$$\frac{p}{P_C} = \frac{\lambda}{n\mu} = \rho \qquad (9)$$

Eq (9) reveals an elegant simplicity: the ratio of the fixture $p$-value to its limiting value at congestion matches the ratio of arrival rate to service rate at the fixture. In queueing theory, the ratio of arrival rate to service rate occurs often and is known as the **utilization factor**, universally designated as "$\rho$". It provides a measure of the average use of the server.

The conditions implicit in Eqs (7), (8) and (9) are summarized in Table 9 and portrayed as the dimensionless ramp function on the unit square in Figure 39. An example application of the dimensionless ramp function is provided in the next section of this report.

**Table 9.** Summary of Expressions for Fixture $p$-values on the Unit Square.

| Utilization Factor* | Design Condition | Expression for Fixture $p$-value | Location in Fig 39 Unit Square | Equation Number |
|---|---|---|---|---|
| $0 \le \rho \le 1$ | No queueing expected | $p = \rho P_C$ | On the ramp | (7) or (10a) |
| $\rho > 1$ | Congestion, queueing occurs | $p = P_C$ | On the plateau | (8) or (10b) |

*Besides the result give in Eq (9), some alternate expressions for the dimensionless utilization, factor in the context of premise plumbing, are:

$$\rho = \frac{\lambda}{n\mu} = \frac{NT_0}{nT} = \frac{N}{N_{MAX}}$$

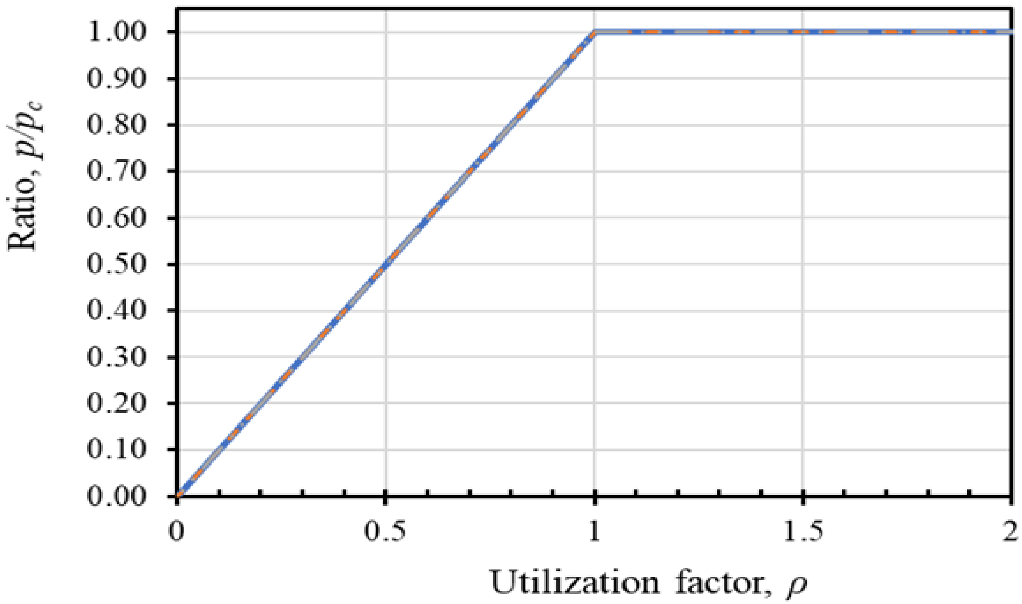


**Fig. 39.** Dimensionless Ramp Function on the Unit Square (Fixture Probability-Utilization Plot).

Table 10 lists average fixture occupancy times for a small sample of buildings in the US, Japan and Taiwan. Men and women engage fixtures for different durations. While observations are fairly consistent for different types of buildings at multiple geographical locations, more data are needed to broaden coverage.

**Table 10.** Fixture Occupancy Times in Different Types of Buildings.

| Building Type | Fixture | $T_O$, Average Occupancy Time (seconds) | | | Reference |
|---|---|---|---|---|---|
| | | Men | Women | Ward | |
| Office, USA | Water Closet | 85 | 88 | - | [16] |
| | Lavatory | 18 | 52 | - | |
| Office, Japan | Water Closet | 260 | 110 | - | [17] |
| | Lavatory | 12 | 17 | - | |
| | Urinal | 37 | - | - | |
| Hospital, Outpatient and Staff, Japan | Water Closet | 260 | 110 | 110 | [18] |
| | Lavatory | 15 | 30 | 30 - 40 | |
| | Shower | - | - | 480 | |
| | Medical Sink | - | - | 35 | |
| Hotel Guest Room, Japan | Wash basin | 230 | | - | [19] |
| | Shower | 160 | | - | |
| | Bathtub | 315 | | - | |
| | Public Shower [a] | 420 | | - | |
| Train Station | Water Closet, Taiwan | 34 | 71 | - | [20] |
| | Water Closet, Japan | 30 - 35 | 90 - 93 | - | |

[a] Large banks of shower heads, including washbasin

## 4.3. Simulating the Ramp Function

Applying principles from queueing theory, a Monte Carlo exercise was performed to simulate the steady-state operation of a restroom. The purpose of the simulation was to explore and verify the properties of the dimensionless ramp function shown in Figure 39. In the queueing exercise, customers arrive at random according to a Poisson process, receive service for a certain length of time and then depart the system. When dealing with premise plumbing, the service time is the same as the fixture occupancy time. Historically, Konen [15, 16] proposed principles from queueing theory to determine fixture count requirements for office buildings based on service population and occupancy times.

Figure 40 is a definition sketch for the queueing exercise. The operation of a restroom with *n* fixtures (urinals) was simulated as a *M/D/n* queue process. *M* denotes an exponential probability distribution for Poisson arrivals and *D* denotes a deterministic service rate. The busy time for the flush valve urinals was set at a fixed pulse duration, $\tau$=5 s. For this simulation exercise, the waiting time is unlimited so that no customer is lost. If a customer arrives and all fixtures are occupied, the customer waits in line as long as necessary for the next available fixture. The program tracked the total duration of water flow at all fixtures under steady-state conditions (*i.e*., arrivals ≡ departures).

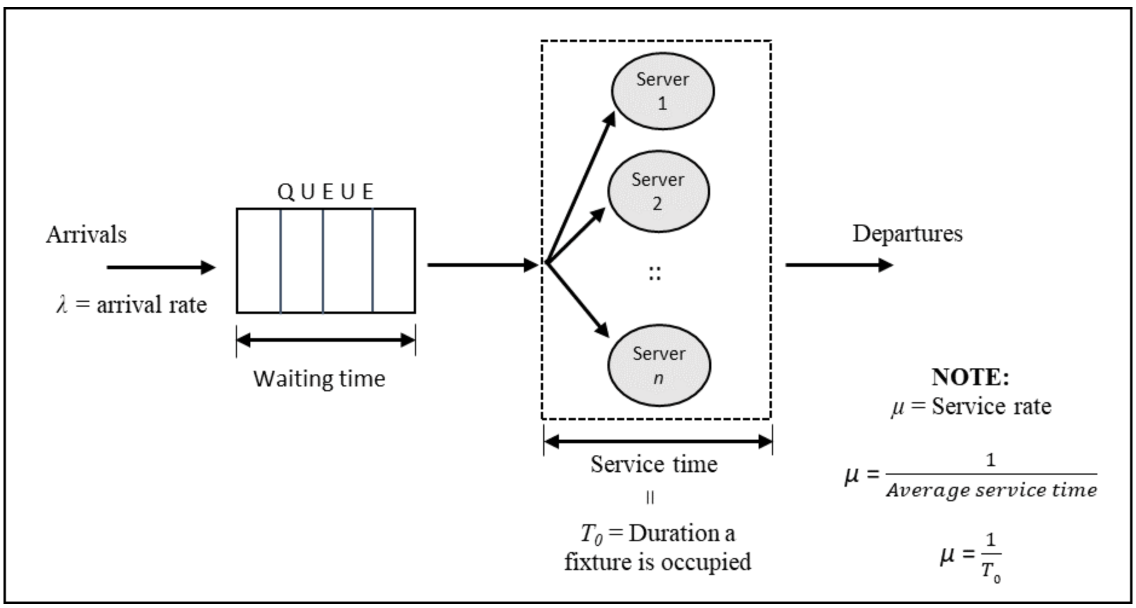


**Fig. 40.** Definition Sketch for Queueing Theory Applied to Plumbing Fixture Use.

Fixture *p*-values from the simulation were calculated with Eq (3); the utilization factor was computed as $\rho=\lambda/n\mu$, per Eq (9). Figure 41 shows *p*-value versus $\rho$ for 12 cases: three occupancy times ($T_O$ = 60, 90, 120 s) each with four fixture counts ($n$ = 1, 2, 5, 10 urinals). The 12 cases appear as a trio of color-coded lines (orange, blue or black). This behavior is expected since points having common colors share a common occupancy time and, according to Eq (10a) in Table 9, will ramp up from zero to the same limiting *p*-value at congestion, $P_C = \mu\tau = \tau/T_O$. Each point in Figure 41 represents the average of 1 000 Monte Carlo simulations of the queueing process depicted in Figure 40.

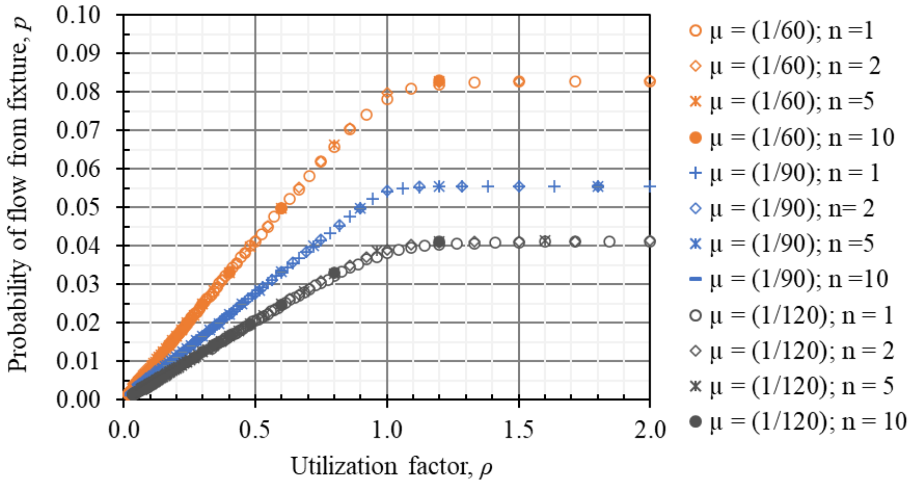


**Fig. 41.** Dimensionless ($p$)||($\rho$) diagram; Probability Plateau Occurs at Congestion.

Some key take-away points about Figure 41 are as follows:

● Emergence of the fixture *p*-value plateau at congestion is evident. The computed $P_C$ values agree exactly with the predictions from Eq (8). For instance, the black line with fixture occupancy time of $T_O$ = 120 s has $P_C = \tau/T_O$ = 5/120 = 0.042 just as shown in the plateau region of Figure 41.

● In the region where ρ<1, Eq (7) is valid. The linear growth in fixture *p*-values with $\rho=\lambda/n\mu$ is a direct result of an increasing arrival rate (since the denominator in $\rho$ is fixed in a given simulation).

● In the region where ρ>1, Eq (8) controls. The fixture *p*-values have reached their upper bound, indicating congestion is prevalent (*i.e.,* queues are common).

● When ρ=1, the arrival rate equals the service rate for all *n* fixtures. The ramp response meets the congestion plateau. The probability of fixture use is maximized and congestion is imminent.

● Reducing fixture occupancy time leads consistently to higher fixture *p*-values for a given $\rho$ (see orange line above blue line above black line). This happens because as $T_O$ decreases, there is greater fixture availability to other users, hence, increasing the chances of flow at the fixture.

Figure 41 is an intermediate step on the path to develop the dimensionless ramp function depicted in Figure 39. The 12 cases in Figure 41 are a very small sample of the results that could be generated for different fixtures under different use conditions. Fortunately, there is no need to recreate Figure 41 for each new situation. Instead, a universal ramp function can be prepared to encompass all possible scenarios. It is generated by rescaling the *p*-values on the *y*-axis in Figure 41 by their corresponding congestion probability ($P_C = \tau/T_O$). This operation collapses the trio of lines in Figure 41 to the single dimensional ramp function on the unit square, shown in Figure 39.

Figure 39 can provide guidance to engineers who seek a fixture *p*-value for premise plumbing design. To illustrate, consider a flush valve urinal in the community center of a proposed residential development. Suppose the engineer determines the flow duration is τ=3 s (from fixture manufacturer) and $T_O$ = 60 s (from experience). It follows immediately that the upper bound on the *p*-value is $P_C$ = 3/60 = 0.05 (from Eq 8). At this point, the engineer exercises professional judgment (or queries AI) and ultimately selects a utilization factor $\rho$=0.75. This leads to a flush valve urinal *p*-value of (0.75)(0.05) = 0.0375 for the new building.

### 4.4. Results and Discussion

The peak period probability of men's room lavatory use for the data described in Section 4.1 was found using Eq. (3) with $n$=2. The peak period was the hour with the maximum number of water use events. Each day the peak hour was determined and the corresponding $p$-value was calculated. Figure 42 shows that over the 23-day period, lavatory $p$-values vary by an order of magnitude, ranging from a minimum of 0.024 to a maximum of 0.274 with an overall average of 0.086. These lavatory sinks are manually operated; therefore, the user controls the duration of flow at the fixture.

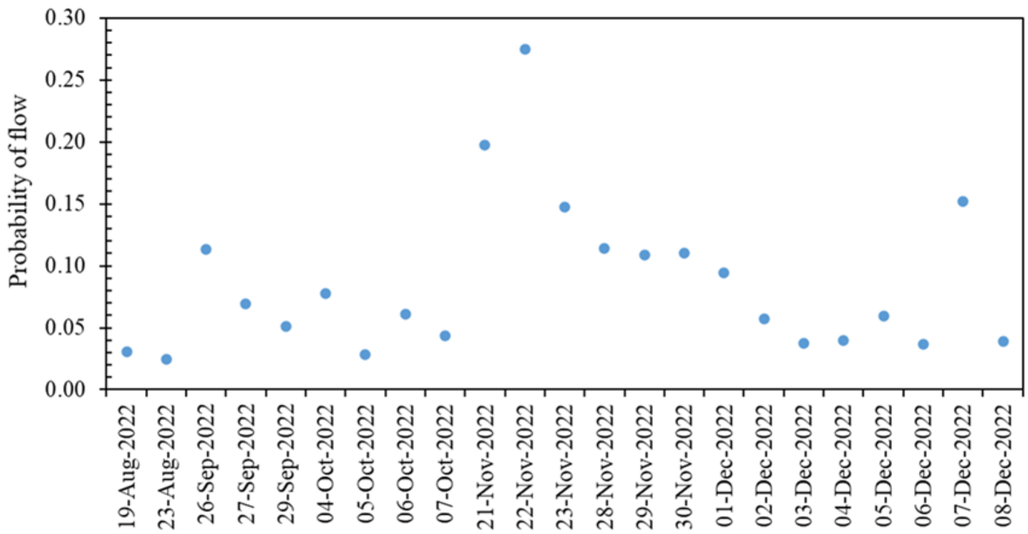


**Fig. 39.** Daily Peak Hour Probability of Men's Room Lavatory Sink Use at MSH Cafeteria.

To smooth the plot in Figure 42, a cumulative running average of the daily peak probability of use was computed (Figure 43). About half way through the data set, the running average for the lavatory $p$-value stabilized in the range of 0.08 to 0.10. The high variability in the raw data underscores the importance of getting large samples to tighten confidence bands on results.

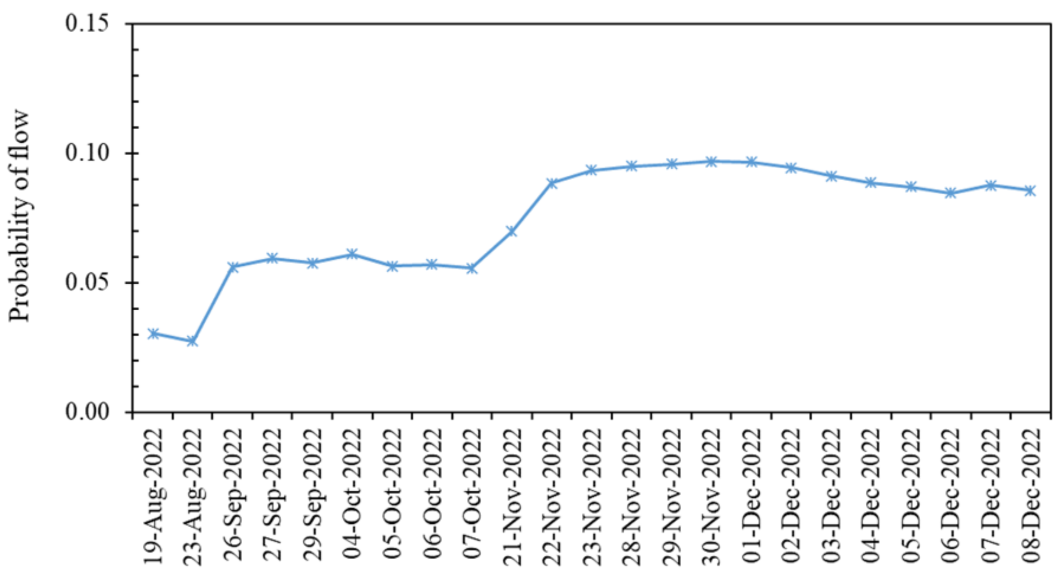


**Fig. 40.** Cumulative Running Average of Fixture $p$-values shown in Figure 42.

# 5. Task 3: Data Management Plan

The availability of open research data encourages the collaborative networking of researchers, private sectors, and citizens to contribute and participate in tackling issues such as predicting water demand. It also offers opportunities to test hypotheses, replicate research, and avoid duplication of effort [22]. This section provides details of the data collected in the data dictionary, the data description, and the data location. The availability of this dataset encourages a cooperative effort between researchers and private entities to create a global database of fixture *p*-values.

## 5.1. Data Dictionary

The data dictionary contains information about a database. The database created from the data collection activities detailed in Section. 3.4.3.4 contains several files differentiated by location. The files are named according to the following naming convention:

*StartDate_EndDate (MMDDYYYY)_Building_Location_FixtureType_NumberofFixtures*,

For example, consider the file name,

*08192022_10072022_MarianSpencerCafeteria_MensRestroom_Lavatory_2*.

This file contains data collected from two lavatory sinks in the men's restroom of the cafeteria at Marian Spencer Hall during the period August 19, 2022 through October 7, 2022.

As summarized in Table 11, five types of information are contained in the database file. Figure 44 is a snapshot of one of the files in the database and shows five columns, one for each of the five types of collected information.

**Table 11.** Details in the .csv Data Files.

| Field Number | Field Name | Data Type | Field Size for display | Description | Example |
|---|---|---|---|---|---|
| **[1]** | **EventNumber** | Integer | 10 | Unique ID of each date | 1 |
| **[2]** | **Date** | Date | 10 | Date of data collection | 8/19/2022 |
| **[3]** | **EventStartTime** | Time | 10 | Start time of flow | 10:54:48 AM |
| **[4]** | **EventEndTime** | Time | 10 | End time of flow | 10:55:13 AM |
| **[5]** | **Duration_sec** | Integer | 10 | Duration of flow measured by the sensor | 24.75 |

A README.txt file explains the purpose and contact information of the owner of the database. A MATLAB (R2021a) script (MSHRestroom_Pvalue.docx) was written to analyze the data to calculate the fixture probability of use. The data collection template is included in Appendix B.

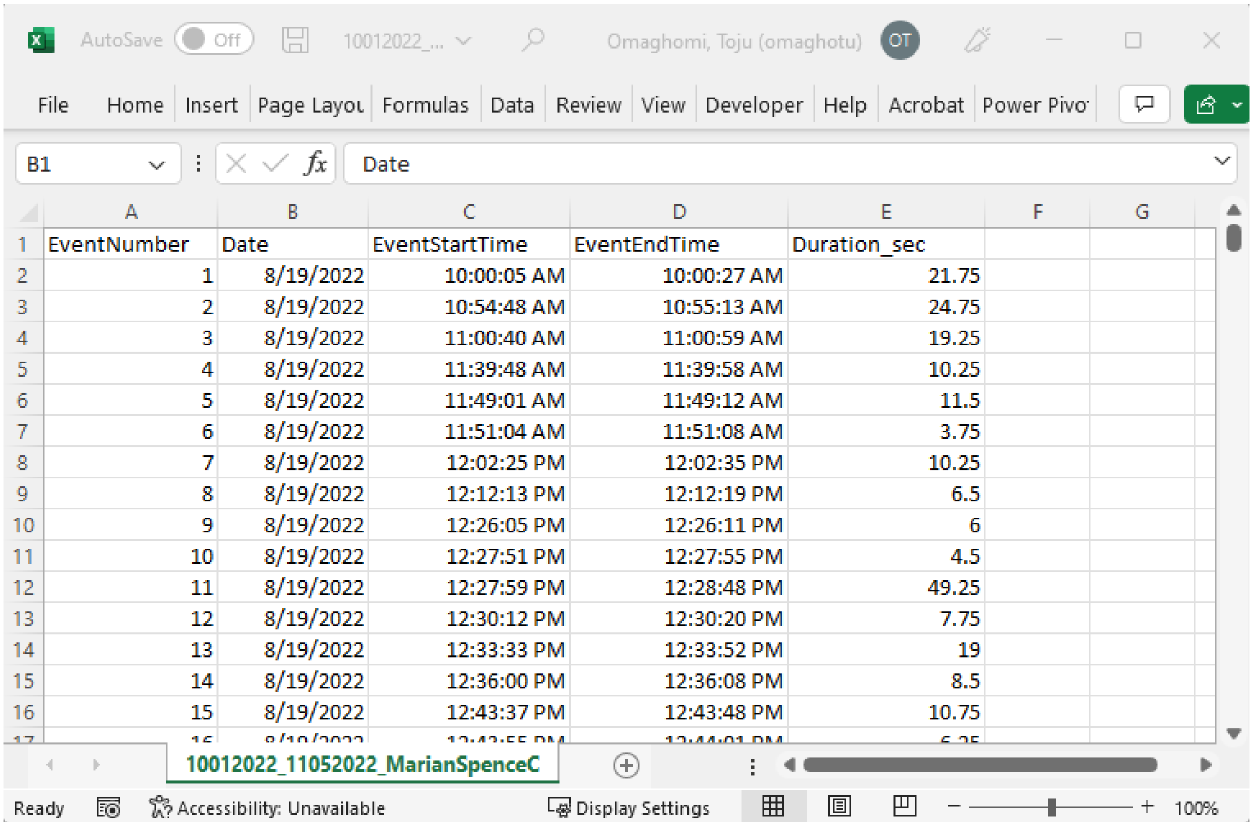

| EventNumber | Date | EventStartTime | EventEndTime | Duration_sec |
|---|---|---|---|---|
| 1 | 8/19/2022 | 10:00:05 AM | 10:00:27 AM | 21.75 |
| 2 | 8/19/2022 | 10:54:48 AM | 10:55:13 AM | 24.75 |
| 3 | 8/19/2022 | 11:00:40 AM | 11:00:59 AM | 19.25 |
| 4 | 8/19/2022 | 11:39:48 AM | 11:39:58 AM | 10.25 |
| 5 | 8/19/2022 | 11:49:01 AM | 11:49:12 AM | 11.5 |
| 6 | 8/19/2022 | 11:51:04 AM | 11:51:08 AM | 3.75 |
| 7 | 8/19/2022 | 12:02:25 PM | 12:02:35 PM | 10.25 |
| 8 | 8/19/2022 | 12:12:13 PM | 12:12:19 PM | 6.5 |
| 9 | 8/19/2022 | 12:26:05 PM | 12:26:11 PM | 6 |
| 10 | 8/19/2022 | 12:27:51 PM | 12:27:55 PM | 4.5 |
| 11 | 8/19/2022 | 12:27:59 PM | 12:28:48 PM | 49.25 |
| 12 | 8/19/2022 | 12:30:12 PM | 12:30:20 PM | 7.75 |
| 13 | 8/19/2022 | 12:33:33 PM | 12:33:52 PM | 19 |
| 14 | 8/19/2022 | 12:36:00 PM | 12:36:08 PM | 8.5 |
| 15 | 8/19/2022 | 12:43:37 PM | 12:43:48 PM | 10.75 |

**Fig. 44.** Data File

## 5.2. Data Repository

The raw and analyzed data will be documented and organized using the Dublin Core metadata schema and archived on Scholar@UC. The database will be stored in the hard drives of university-owned computers and backed up automatically to an on-campus research data-secured backup service provided by the university and an online secured data storage service provided by the university through Microsoft OneDrive service. The backup service and online storage data can be maintained as long as needed without limitation. The database is open-access, discoverable, and available for download. For questions on the data, contact Steven Buchberger.

# 6. Water Demand Calculator: Recent Developments, Validating Data

The WDC was developed in 2018 to estimate peak water demand in residential buildings. It is a Microsoft Excel file that uses macros to select a suitable method of estimating peak demand based on the user's input. WDC selects from one of three methods to estimate peak indoor water demand: 1) Exhaustive Enumeration (ExEn), 2) Modified Wistort's Method (MWM), and 3) Wistort's Method (WM) [23]. The current version of the WDC is hosted on the IAPMO website.

## 6.1. Recent Developments

Since its initial release in 2018, the WDC has been revised several times increase speed and improve transitions between algorithms. As shown in Table 12, a convolution method has replaced exhaustive enumeration in version 2.2. Like the ExEn method, convolution directly evaluates combinations of busy fixtures. However, convolution tends to be faster needing $\prod_k (n_k + 1)$ calculations compared $2^N$ calculations for ExEn. Here $N$ is the total number of fixtures. The convolution method analyzes the combinations of busy fixtures within each fixture group before combining different fixture groups. This strategy reduces the number of computation steps required to arrive at the 99$^{\text{th}}$ percentile. Figure 45 illustrates the transitions between algorithms.

**Table 12**. Transition Criteria for WDC Version 2.1 and 2.2.

| Current WDC v 2.1 | | Updated WDC v 2.2 | |
|---|---|---|---|
| **Method/Algorithm** | **Selection criteria** | **Method/Algorithm** | **Selection criteria** |
| Exhaustive Enumeration | $N \le 30$ | Convolution | Calculation steps ≤ 1,000,000 **AND** $H \le 1$ |
| Modified Wistort's Method | $N > 30$ **AND** $H < 5$ | Modified Wistort's Method | Calculation steps > 1,000,000 **OR** $1 < H < 5$ |
| Wistort's Method | $H \ge 5$ | Wistort's Method | $H \ge 5$ |

Note: $H = \sum_{k=1}^{K} n_k p_k$ . Hunter number is the average number of simultaneous busy fixtures during peak water use.

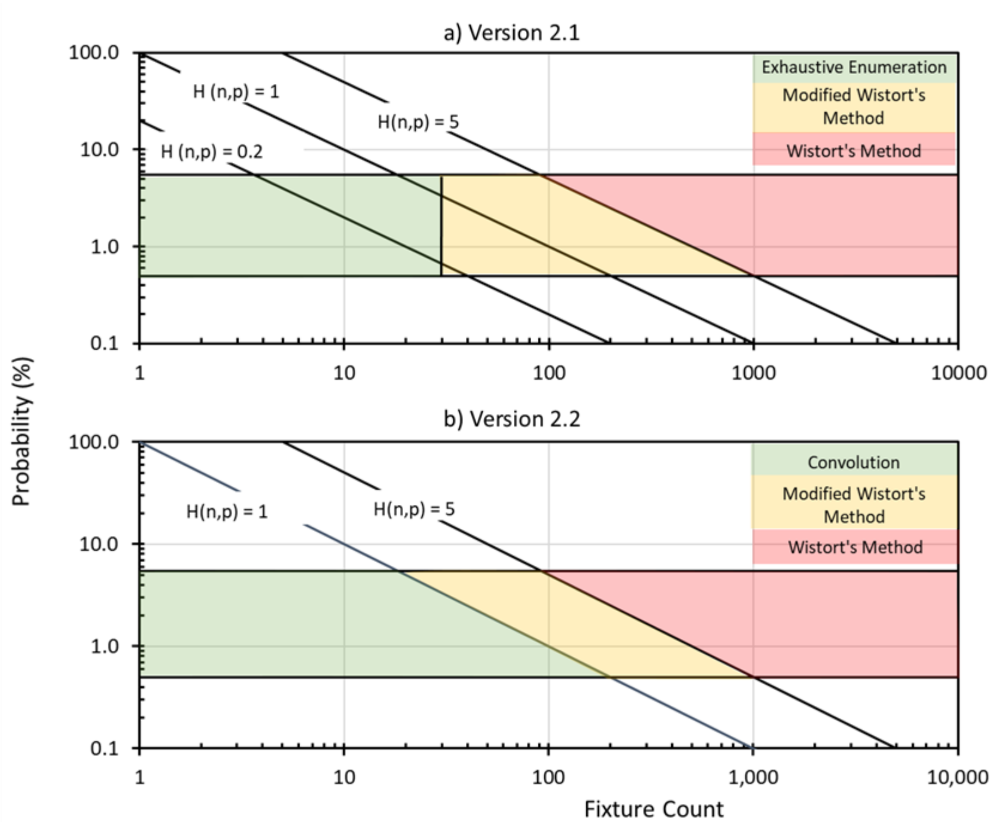


**Fig. 45.** Transition Criteria for WDC Versions 2.1 and 2.2.

## 6.2. Field Verification of the WDC

The California Building Standards Commission (CBSC) was petitioned to adopt Appendix M-Peak Water Demand Calculator (WDC) of the 2021 Uniform Plumbing Code (UPC) into the California Plumbing Code (CPC). In preparation for this petition, measurements of peak flow rate from hot water use in 20 apartment buildings were gathered and compared to the predictions made by following Appendix A of the UPC/CPC and Version 2.1 of the WDC. Below is a summary of the results.

Figure 46 (top) shows data for 20 multifamily buildings ranging from 8 to 384 apartments. The black dots (measured 99th percentile peak flow rates) are near the x-axis and are significantly lower than the peak demand estimated by the UPC/CPC. Figure 46 (bottom) zooms in on the cluster of 16 buildings with fewer than 300 Water Supply Fixture Units (WSFU). In each case, the actual measured peak demands are much lower than the UPC/CPC estimates. Actual peak flow rates mean the 99th percentile of non-zero flows for all data collected over the entire monitoring period.

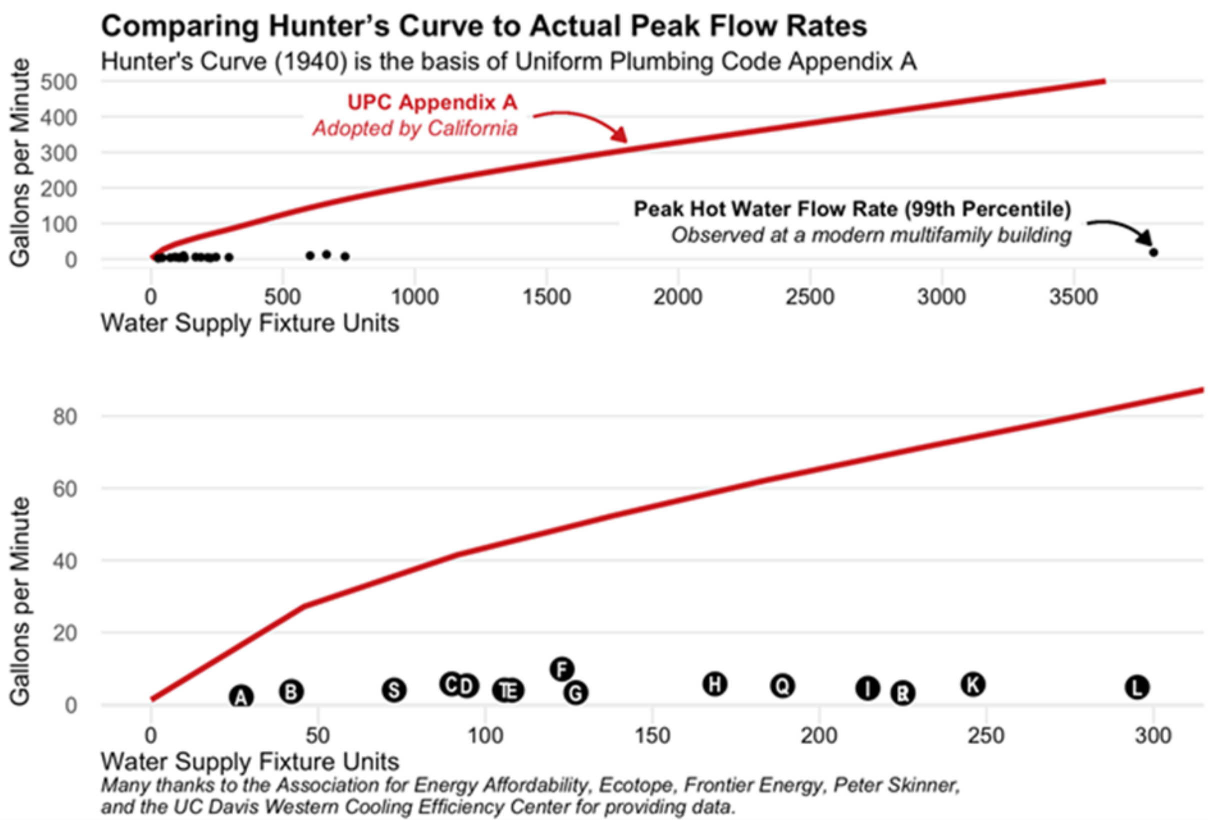


**Fig. 46.** Comparing UPC Appendix A (Hunter's curve) to Actual Peak Flow Rates in Multifamily Buildings.

Figure 47 presents data for the 20 multifamily buildings included in the study. Monitoring periods ranged from 9 days to over 2 years, and logging intervals ranged from 1 to 60 seconds. Buildings are ordered by UPC Appendix A design flow value. UPC Appendix A flow values for buildings M, N, O, and P are out of scale and are not included in this figure.

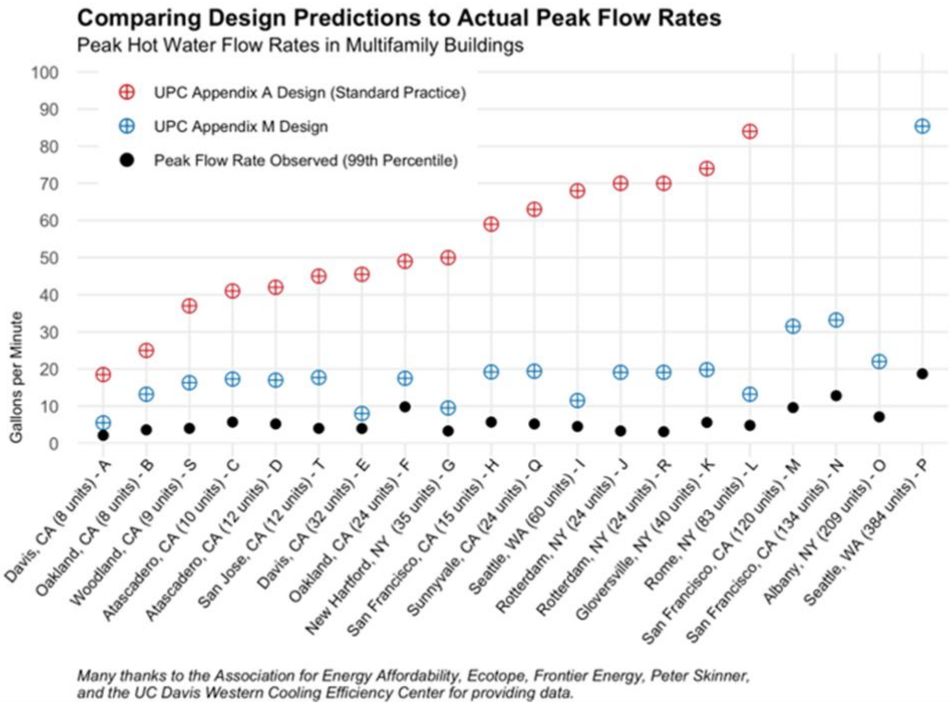


**Fig. 47.** Comparing Design Predictions to Actual Peak Flow Rates.

Table 13 summarizes the detailed data used to prepare Fig. 47. Study Peak is the 99th percentile of non-zero hot water flow rates observed during the monitoring period. The percentage time with zero flow is not displayed, where monitoring issues may have impacted the accuracy of the metric. For building P, the WSFUs exceed the UPC Appendix A design curve; the last value on the design curve was used.

**Table 13.** Summary of the Detailed Data for the Analyzed Multifamily Buildings.

| | | | *Monitoring Data* | | | | *UPC Appendix M* | | *UPC Appendix A* | | |
|---|---|---|---|---|---|---|---|---|---|---|---|
| | City | Monitored Apartments | Monitoring Period (day) | Logging Interval (sec) | Time at Zero Flow | Study Peak (gpm) | Design (gpm) | Design Relative to Study Peak | WSFU | Design (gpm) | Design Relative to Study Peak |
| A | Davis, CA | 8 | 304 | 15 | 87% | 2.1 | 6 | 2.6x | 27 | 19 | 8.8x |
| B | Oakland, CA | 8 | 10 | 1 | - | 3.6 | 13 | 3.7x | 42 | 25 | 6.9x |
| C | Atascadero, CA | 10 | 257 | 60 | - | 5.7 | 17 | 3.0x | 90 | 41 | 7.2x |
| D | Atascadero, CA | 12 | 257 | 60 | - | 5.2 | 17 | 3.3x | 95 | 42 | 8.1x |
| E | Davis, CA | 32 | 304 | 15 | 56% | 4.0 | 8 | 2.0x | 108 | 46 | 11.5x |
| F | Oakland, CA | 24 | 14 | 1 | 48% | 9.8 | 18 | 1.8x | 123 | 49 | 5.0x |
| G | New Hartford, NY | 35 | 26 | 60 | 69% | 3.3 | 10 | 2.9x | 127 | 50 | 15.2x |
| H | San Francisco, CA | 15 | 9 | 1 | - | 5.7 | 19 | 3.4x | 169 | 59 | 10.4x |
| I | Seattle, WA | 60 | 823 | 60 | - | 4.5 | 12 | 2.6x | 215 | 68 | 15.1x |
| J | Rotterdam, NY | 24 | 18 | 60 | 38% | 3.3 | 19 | 5.8x | 225 | 70 | 21.2x |
| K | Gloversville, NY | 40 | 12 | 60 | - | 5.6 | 20 | 3.5x | 246 | 74 | 13.2x |
| L | Rome, NY | 83 | 15 | 60 | 37% | 4.8 | 13 | 2.8x | 295 | 84 | 17.5x |
| M | San Francisco, CA | 120 | 12 | 1 | - | 9.6 | 32 | 3.3x | 603 | 143 | 14.9x |
| N | San Francisco, CA | 134 | 12 | 1 | 38% | 13 | 33 | 2.6x | 665 | 155 | 12.1x |
| O | Albany, NY | 209 | 21 | 60 | - | 7.1 | 22 | 3.1x | 735 | 168 | 23.6x |
| P | Seattle, WA | 384 | 609 | 60 | 8% | 19 | 85 | 4.6x | 3802 | 500 | 26.7x |
| Q | Sunnyvale, CA | 24 | 272 | 60 | - | 5.4 | 19 | 3.7x | 189 | 63 | 12.1x |
| R | Rotterdam, NY | 24 | 22 | 1 | - | 3.1 | 19 | 6.2x | 225 | 70 | 22.6x |
| S | Woodland, CA | 9 | 128 | 60 | 84% | 4 | 16 | 4.1x | 73 | 37 | 9.3x |
| T | San Jose, CA | 12 | 59 | 60 | 72% | 4 | 18 | 4.4x | 106 | 45 | 11.3x |
| | | | | | | | **Median** | **3.3x** | | | **12.1x** |

Table 14 provides the metadata and fixture counts for the 20 apartment buildings located in California, New York, and Washington. Occupancy types included low-income, market rate, senior and mixed.

**Table 14.** Summary of Fixture Counts for the Analyzed Multifamily Buildings.

| | City | Monitored Apartments | Occupancy Type | Combo Bath /Shower | Lavatory Faucet | Shower | Water Closets | Dish-washer | Kitchen Faucet | Clothes Washer | Total Fixtures |
|---|---|---|---|---|---|---|---|---|---|---|---|
| A | Davis, CA | 8 | MF Low Income | 0 | 8 | 8 | 8 | 0 | 8 | 0 | 32 |
| B | Oakland, CA | 8 | MF Market Rate (Rent Controlled) | 8 | 8 | 0 | 8 | 0 | 8 | 1 | 33 |
| C | Atascadero, CA | 10 | MF Low Income | 18 | 18 | 0 | 18 | 10 | 10 | 0 | 74 |
| D | Atascadero, CA | 12 | MF Low Income | 18 | 18 | 0 | 18 | 12 | 12 | 0 | 78 |
| E | Davis, CA | 32 | MF Low Income | 0 | 32 | 32 | 32 | 0 | 32 | 0 | 128 |
| F | Oakland, CA | 24 | MF Market Rate | 24 | 24 | 0 | 24 | 0 | 24 | 2 | 98 |
| G | New Hartford, NY | 35 | MF Senior | 0 | 35 | 35 | 35 | 0 | 35 | 3 | 143 |
| H | San Francisco, CA | 15 | MF Low Income | 24 | 24 | 0 | 24 | 15 | 15 | 15 | 117 |
| I | Seattle, WA | 60 | MF Senior Low Income | 0 | 60 | 60 | 60 | 0 | 60 | 4 | 244 |
| J | Rotterdam, NY | 24 | MF Net Zero (Mixed Occupancy) | 24 | 28 | 4 | 28 | 24 | 24 | 24 | 156 |
| K | Gloversville, NY | 40 | MF Low-and-Moderate Income | 40 | 40 | 0 | 40 | 40 | 40 | 2 | 202 |
| L | Rome, NY | 83 | MF Senior | 0 | 83 | 83 | 83 | 0 | 83 | 5 | 337 |
| M | San Francisco, CA | 120 | MF Low Income | 120 | 120 | 0 | 120 | 0 | 120 | 6 | 486 |
| N | San Francisco, CA | 134 | MF Low Income | 134 | 134 | 0 | 134 | 0 | 134 | 4 | 540 |
| O | Albany, NY | 209 | MF Senior | 0 | 209 | 209 | 209 | 0 | 209 | 10 | 846 |
| P | Seattle, WA | 384 | MF Market Rate | 454 | 565 | 0 | 565 | 384 | 384 | 384 | 2,736 |
| Q | Sunnyvale, CA | 24 | MF Low Income | 36 | 36 | 0 | 36 | 24 | 24 | 0 | 189 |
| R | Rotterdam, NY | 24 | MF Net Zero (Mixed Occupancy) | 24 | 28 | 4 | 28 | 24 | 24 | 24 | 156 |
| S | Woodland, CA | 9 | MF Low Income | 14 | 14 | 0 | 14 | 9 | 9 | 0 | 46 |
| T | San Jose, CA | 12 | MF Low Income | 21 | 21 | 0 | 21 | 12 | 12 | 0 | 66 |

The data presented in Fig. 47 and Tables 13 and 14 are for hot water flow rates. The reason is that the investigators providing the measured flow rates were focused on the performance of hot water systems.

What happens when cold water demand is included? Figure 48 presents the cumulative distribution of observed flow rates in Building R (represented by dots, with a vertical solid line indicating the study peak flow rate of each flow type). It compares those observed values with design UPC Appendix M values (vertical dashed lines to the far right). The total flow was calculated by adding the hot and cold-water flow data. The comparison shows that UPC Appendix M is a conservative estimator of peak water flow rates for hot, cold, and total water flow.

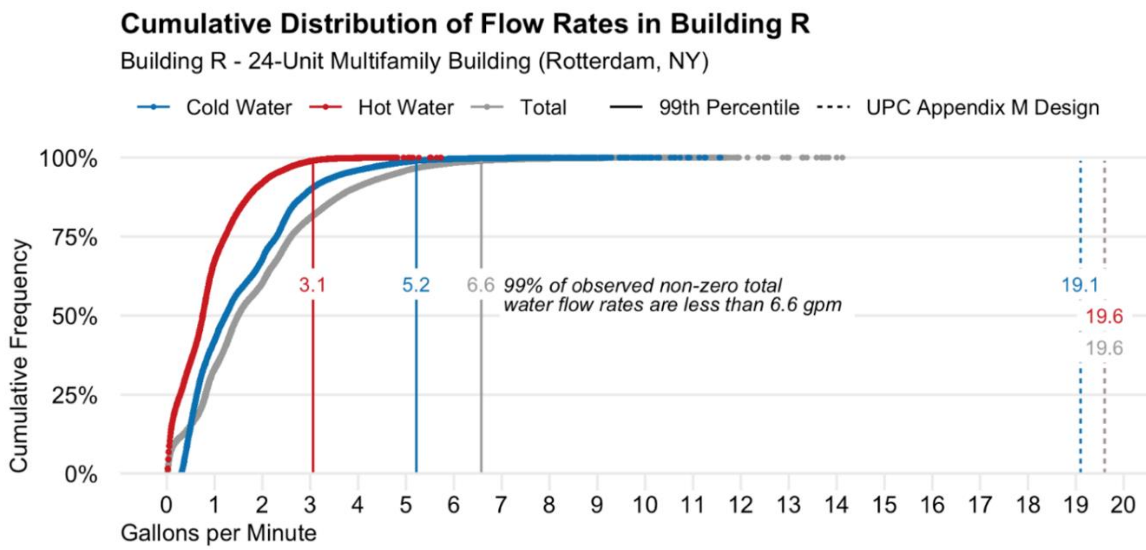


**Fig. 48.** Cumulative Distribution of Flow Rates in Building R.

A right-sized plumbing design aims to avoid issues from oversizing pipes and equipment, including wasted building materials, inaccurate water meter measurements, increased time-to-tap, and water residence times large enough to allow bacterial growth. It also aims to avoid issues from under-sizing, such as user dissatisfaction with low flow rates. In his seminal work on rightsizing for expected plumbing demand load, Roy Hunter [1] proposed to calculate the design flow rate as the flow rate with a specific probability of being exceeded. Hunter accepted that 1% of flows in a "congested condition of service" period could be expected to exceed his peak flow rate estimate. UPC Appendix M adapts this methodology, providing updated probabilities of fixture use and estimates the 99$^{th}$ percentile flow rate in the single hour with the highest cumulative demand of water by volume. We refer to this hour of maximum volume as the "peak hour" and the predicted 99$^{th}$ percentile within that population of flow rates as the "peak hour demand."

A different approach was taken in the analysis of the data presented above. It looked at the 99$^{th}$ percentile of non-zero flows over the entire monitoring period, which we call the "peak flow rate," or when necessary to differentiate from other predictive metrics, the "study peak flow rate."

Comparing these two approaches across buildings shows that neither metric consistently exceeded the other. In the 20 multifamily buildings in our sample, the study peak flow rate was observed to measure from 4.5 gpm above to 3.0 gpm below the peak hour metric, with a median of 0.7 gpm below. Neither metric was above that predicted by Appendix M. Table 15 displays these two metrics alongside the UPC Appendix M design value, with the study peak highlighted in yellow when it exceeded the peak hour demand.

**Table 15.** Comparison of Two Metrics to Assess Peak Water Flows in Multifamily Buildings.

| Building | City | Monitored Apartments | Monitoring Period (days) | Peak Hour (24h) | *Peak flow observed in* | | UPC App. M Design (gpm) |
|---|---|---|---|---|---|---|---|
| | | | | | Peak Hour (gpm) | Study (gpm) | |
| **A** | Davis, CA | 8 | 304 | 18 | 2.1 | 2.1 | 6 |
| **B** | Oakland, CA | 8 | 10 | 11 | 3.5 | 3.6 | 13 |
| **C** | Atascadero, CA | 10 | 257 | 17 | 6.4 | 5.7 | 17 |
| **D** | Atascadero, CA | 12 | 257 | 16 | 6.0 | 5.2 | 17 |
| **E** | Davis, CA | 32 | 304 | 11 | 3.9 | 4.0 | 8 |
| **F** | Oakland, CA | 24 | 14 | 21 | 12.5 | 9.8 | 18 |
| **G** | New Hartford, NY | 35 | 26 | 9 | 4.2 | 3.3 | 10 |
| **H** | San Francisco, CA | 15 | 9 | 7 | 4.5 | 5.7 | 19 |
| **I** | Seattle, WA | 60 | 823 | 9 | 5.2 | 4.5 | 12 |
| **J** | Rotterdam, NY | 24 | 18 | 9 | 3.8 | 3.3 | 19 |
| **K** | Gloversville, NY | 40 | 12 | 8 | 6.5 | 5.6 | 20 |
| **L** | Rome, NY | 83 | 15 | 10 | 5.0 | 4.8 | 13 |
| **M** | San Francisco, CA | 120 | 12 | 18 | 11.6 | 9.6 | 32 |
| **N** | San Francisco, CA | 134 | 12 | 18 | 15.8 | 13.0 | 33 |
| **O** | Albany, NY | 209 | 21 | 0 | 2.6 | 7.1 | 22 |
| **P** | Seattle, WA | 384 | 609 | 20 | 20.9 | 19.0 | 85 |
| **Q** | Sunnyvale, CA | 24 | 272 | 20 | 7.0 | 5.4 | 19 |
| **R** | Rotterdam, NY | 24 | 22 | 13 | 3.1 | 3.1 | 19 |
| **S** | Woodland, CA | 9 | 128 | 3 | 3.0 | 4.0 | 16 |
| **T** | San Jose, CA | 12 | 59 | 4 | 5.0 | 4.0 | 18 |

The “Peak Hour” metric calculates the 99$^{th}$ percentile of non-zero flow rates within a single peak hour. The “Study” metric calculates the 99$^{th}$ percentile of non-zero flow rates over the entire monitoring period.

Water use data from ten buildings in Michigan were analyzed to extract the measured peak water demand and compare them to estimates of peak water demand from using the WDC. Four out of the ten buildings had details of their fixture count, two hotels, one senior housing, and one office building. Since the current WDC has options for single-family and multi-family fixture *p*-values, the peak demand estimates were calculated using both options for the hotel and the senior housing building. Table 16 summarizes the building details and the peak demand estimates measured and predicted using the WDC and the UPC WSFU.

**Table 16.** Other Buildings with Measured Data Compared to the WDC.

| S/N | Building Type | Location | Number of Floors | Logging Interval (seconds) | Monitoring period (days) | Measured Peak Hour 99th Percentile (gpm)[c] | Measured Maximum Daily flow (gpm) | UPC Design flow (gpm) | WDC 99th Percentile Estimate (gpm) | Comments |
|---|---|---|---|---|---|---|---|---|---|---|
| 1 | Office | Troy, MI | 7 | 60 | 7 | 57.4 | 77.8 | - | - | No fixture details |
| 2 | Hotel | Troy, MI | 17 | 30 | 12 | 89.4 | 115.3 | 344.4 | 34.7[a] / **112.3[b]** | 350 units; 1067 fixtures |
| 3 | Multi-family senior living | Jackson, MI | 6 | 60 | 7 | 17 | 21.7 | 220.9 | **23.3[a]** / 64.8[b] | 180 units; 546 fixtures |
| 4 | Hotel | Birmingham, MI | 6 | 60 | 12 | 55.4 | 74.8 | 193.7 | 21[a] / **55.8[b]** | 150 units; 450 fixtures |
| 5 | Office | Southfield, MI | 25 | 60 | 12 | 9.5 | 19.7 | 204.8 | 19.4[b] | 295 fixtures |
| 6 | Condo | Dearborn, MI | 10 | 60 | 8 | 13.8 | 16.8 | - | - | No fixture details; Hot water only |
| 7 | Not Provided | Ann Arbor, MI | 26 | 60 | 9 | 20.3 | 26 | - | - | No fixture details; Hot water only |
| 8 | Correctional facility | Adrian, MI | - | 120 | 8 | 22.5 | 26 | - | - | No fixture details; Hot water only |
| 9 | Apartment buildings | Kalamazoo, MI | 3 | 60 | 22 | 5.3 | 9.4 | - | - | No fixture details; Hot water only |
| 10 | Apartment buildings | Kalamazoo, MI | 3 | 60 | 13 | 4.8 | 7.5 | - | - | No fixture details; Hot water only |

NOTE: WDC estimates using [a] Multifamily p-values, [b] Single family p-values

[c] the 99th percentile from the non-zero flows measured during the peak hour.

The predicted peak demand estimates for the hotels using the single-family fixture *p*-values were comparable to the measured peak hour 99th percentile flows. In contrast, the measured peak flow in the multi-family senior housing compared well to the predicted peak demand estimates with the multi-family fixture *p*-values. In all four examples with fixture count, the UPC design flow was between 2.6 to 10.4 times the maximum measured flow and 3.5 to 21.6 times the 99th percentile of the measured flow during the study period.

### 6.3. WDC Sensitivity Analysis

In the WDC, three key parameters (*n*, *p*, *q*) are required to compute the 99th percentile demand estimate. Thus far, all fixture *p*-values found from data measurements and used in simulation are less than 0.10; nonetheless, there remains some uncertainty in selecting *p* and *q*-values. A sensitivity analysis reveals how the predicted peak demand changes with an increase or decrease in the input variables *p* and *q*. The sensitivity analysis was performed using the Modified Wistort Method, expressed as

$$Q_{0.99} = \frac{\sum_{k=1}^{K} n_k p_k q_k}{1 - P_0} + (1 + P_0) z_{(0.99)} \sqrt{\frac{(1 - P_0)\sum_{k=1}^{K} n_k p_k (1 - p_k) q_k^2 - P_0 \left(\sum_{k=1}^{K} n_k p_k q_k\right)^2}{(1 - P_0)^2}} \tag{11}$$

where *n, p, q, k* are, respectively, the number of fixtures, probability of fixture use, fixture flow rate, and the number of fixture groups (faucet, shower, etc.), $z_{(0.99)}$ is the 99th percentile of the standard normal distribution and $P_0$ is the probability of stagnation calculated as $\prod_{k=1}^{K}(1-p_k)^{n_k}$.

Figure 49 shows the change in $Q_{0.99}$ for different input values *p* and *q*. The change in peak demand is most sensitive to changes in fixture flow rates. As evident by inspection in Eq (11), the peak demand is proportional to the fixture flow; for instance, if the fixture flow rate is doubled, the estimated demand doubles. The predicted peak flow also varies with fixture *p*-value, but the sensitivity depends on the choice of both *n* and *p*. For instance, $Q_{0.99}$ increases between 20% to 75% when an initial *p*-value between 0.001 to 0.25 is doubled. This increase is magnified slightly when the fixture count increases.

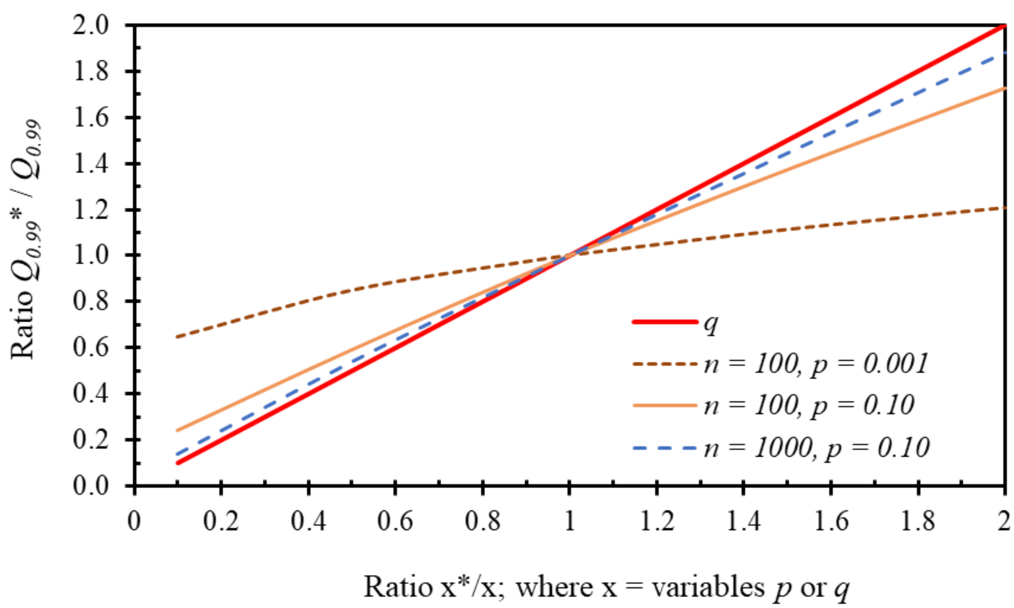


**Fig. 49.** Effect of Changing *p* and *q* on the value of $Q_{0.99}$ computed from Eq. (11) where *k* =1)

NOTE: x* = new input value and $Q_{0.99}$* = changed output value

# 7. Conclusions and Recommendations

- A wireless sensor network with distributed battery-powered, low-cost modules for non-invasive waterflow event detection has been successfully designed, constructed, verified and deployed for collecting high-resolution water usage data at individual fixtures.
- The combination of acoustic and thermal modalities in a non-intrusive low-cost sensor provided confirmation from both sensor modalities in all flow events.
- The new wireless sensor can collect continuous high-resolution data necessary to estimate fixture probability of use.
- The data are collected in a simple format, and the method of estimating fixture *p*-values is easy to follow and implement.
- The predicted peak flow using fixture *p*-values from the observation method is comparable to the measured flow during the peak window showing that the estimated fixture *p*-values from observation is a reliable method of arriving at fixture *p*-values pending data availability.
- Simulating arrivals at fixtures shows that there is a maximum probability of flow at a given fixture depending on the fixture's operational characteristics and user behavior. The maximum probability of use occurs when there is congestion (*i.e*., formation of a queue at a fixture).
- A novel dimensionless unit square ramp function is developed and demonstrated as a versatile approach to help engineers obtain reasonable estimates of fixture *p*-values needed for design of premise plumbing systems in new buildings.
- The estimate of peak water demand is sensitive to both the fixture *p*-value and fixture *q*-value. Fixture *q*-values generally can be obtained from the manufacturer. However, fixture *p*-values depend on human behavior. It is, therefore, important to collect reliable field data so that representative fixture *p*-values can be determined for a broad array of building types.
- Based on the 20 apartment buildings (12 in California, 6 in New York, 2 in Washington) evaluated to date, the Water Demand Calculator is shown to provide more accurate estimates than conventional plumbing design codes of the peak indoor water flow rates in multifamily occupancies. This includes hot, cold, and total indoor water use. The WDC provides a comfortable margin of safety whether the observed 99$^{th}$ percentile peak flow rates are based solely on the peak hour of use or on all hours of flow for the full duration of the study period.
- The single-family option in the drop-down menu of WDC gave excellent agreement between predicted peak demands and measured peak demands in hotels (Table 16). This finding suggests that hotels can be viewed as a collection of studio apartments where water use follows a quasi-synchronized daily schedule during the business week. This correlated collective behavior keeps fixture *p*-values elevated in a hotel setting, in marked contrast to apartment buildings where fixture *p*-values decrease with the number of units because tenants tend to operate independently of each other.
- With proof of concept for the wireless sensor network firmly established, it is recommended that a research project be authorized to deploy this new technology in a variety of commercial and institutional facilities across the US in order to collect and archive field data that will provide the fixture *p*-values needed to estimate instantaneous peak water demand in new buildings, the most important parameter in proper sizing modern premise plumbing systems.

## References

[1] Hunter RB (1940), *Methods of Estimating Loads on Plumbing Systems*, (Rep. No. BMS65, US National Bureau of Standards), Washington DC.
[2] Buchberger SG, Blokker EMJ, Cole DP (2012), *Estimating Peak Water Demands in Hydraulic Systems I – Current Practice*, (in Proceeding of WDSA2012 Symposium), Adelaide, South Australia, Sept 24-27, 2012.
[3] USNCCIB (1974), *Water Distribution and Supply within Buildings: National Research Needs, National Academy of Sciences*, Counterpart Commission to CIB W-62.
[4] Benazzi RV, Guss L, Orend R, Wyly RS, and Konen TP (1976), *Water Requirements and Procedures for Estimating the Demand for Water in Buildings.* (1976 CIBW62 Symposium)
[5] Steele A (1982), *Engineered Plumbing Design*, 2nd edition, (Construction industry Press Elmhurst, Illinois) 267 pages.
[6] Cole DP (2012) *Determining fixture units for high-efficiency fixtures*, (IAPMO).
[7] Buchberger SG, Omaghomi T, Wolfe T, Hewitt T, Cole DP (2017) *Peak Water Demand Study - Probability Estimates for Efficient Fixtures in Single and Multi-Family Residential*, (IAPMO) Available at https://www.iapmo.org/media/3857/peak-water-demand-study-executive-summary.pdf
[8] Omaghomi T, Buchberger SG, Cole DP, Hewitt J. and Wolfe T (2020), *Probability of Water Fixture Use during Peak Hour in Residential Buildings, (*ASCE Journal of Water Resources Planning and Management), 146(5). https://doi.org/10.1061/(ASCE)WR.1943-5452.0001207
[9] Wistort RA (1994), *A new look at determining water demands in building: ASPE direct analytic method*, (Technical Proceedings; ASPE 1994 Convention, American Society of Plumbing Engineers), Kansas City, MO, 17-34.
[10] Herbert K (2020) *Gaining an Accurate Estimate of Water Demand in Buildings*, (Plumbing Engineer), 48(12):42-45.
[11] IAPMO (2018), U*niform Plumbing Code.* (IAPMO), Ontario, CA, Volume 1
[12] IAPMO (2021), U*niform Plumbing Code.* (IAPMO), Ontario, CA, Volume 1
[13] AWWA (*in press*) *M22 Manual of Water Supply Practice: Sizing Water Service Lines and Meters*, Fourth Edition, (American Water Works Association), Denver, CO.
[14] Persily A, Yashar D, Ferretti NM, Ullah T and Healy W (2020) *Measurement Science Research Needs for Premise Plumbing Systems*, NIST Technical Note 2088, U.S. (Department of Commerce), https://doi.org/10.6028/NIST.TN.2088
[15] Konen, TP (1989), *Water Demand Research: Plumbing Fixture Requirement for Buildings*, (Technical Proceedings ASPE convention) pgs. 104-138
[16] Konen, TP (1992), *Plumbing Fixture Requirement for Office Buildings*, (ASPE Research Foundation), Report 92-02 pp. 77
[17] Murakawa S, Ikeda D, Sakamoto K and Takata H (2021) *Verification on the Dynamic Calculation Method for Cold and Hot Water Supply Loads, and a Simple Calculation Method for the Instantaneous Maximum Flow Rates*, (2021 CIB W062 Symposium)
[18] Ikeda D, Murakawa S and Mitsunaga T, (2021), *Estimation of Water Supply Loads in General Hospital by Dynamic Calculation Method*, (2021 CIB W062 Symposium)
[19] Takata H, Shimada S, Murakawa S and Ikeda D (2021), *Calculation of the Loads of Hot Water Consumption in Japanese Hot Spring Hotel*, (2021 CIB W062 Symposium)
[20] Liao WJ, Cheng CL, He KC and Wu MH, (2010), *Investigation of Public Toilet Facility in Minecart Rapid Transit (MRT) Station*, (2010 CIB W062 Symposium), Sydney, Australia

[21] Gross D, and Harris CM (1985) *Fundamentals of Queueing Theory* 2nd Edition, John Wiley, New York, NY
[22] Zuiderwijk A and Spiers H (2019) *Sharing and re-using open data: A case study of motivations in astrophysics,* (International Journal of Information Management), Volume 49, Pages 228-241.
[23] Omaghomi TO (2019), *Estimating Peak Water Demand in Buildings with Efficient Fixtures: Methods, Merits, and Implications*, Doctoral dissertation, (University of Cincinnati),173 p Available at http://rave.ohiolink.edu/etdc/view?acc_num=ucin1562843108109428

# Appendix A. Selected Bibliography

## A.1. Scholarly Output from Project

**Table 17.** List of Publications, Conference Papers, and Presentations.

| S/N | Title | Authors | Event, Place, Date |
|---|---|---|---|
| 1 | The Water Demand Calculator Leaves Home | S. Buchberger | 2021 Virtual Emerging Water Technology Symposium, May 2021 (Online) |
| 2 | National Survey of Fixture use to Improve Estimates of peak Water Demand in Buildings | T. Omaghomi, and S. Buchberger | ASCE EWRI Congress Milwaukee WI, June 2021 (Online) |
| 3 | Reducing Time-to-Tap Is Just the Tip of the Iceberg: Better Floor Plans Lead to Better Performance | Gary Klein | Passive House Accelerator, Tech Tuesdays, (online) June 2021 |
| 4 | Extending the Water Demand Calculator to Commercial and Institutional Buildings | T. Omaghomi, NM. Ferretti, G. Klein, and S. Buchberger | ASPE Tech Symposium, San Diego California, September 2021 |
| 5 | Estimating the probability of use for efficient fixtures in commercial buildings | T. Omaghomi, T. Li, and S. Buchberger | 47th CIB W062 Int. Symposium Water Supply and Drainage for Buildings, Oct. 2021 (Online) |
| 6 | Water Demand Calculator Development | S. Buchberger | WDC Summit, November 2021 (Online) |
| 7 | Basketball Game Day Water Consumption at the University of Cincinnati Fifth Third Arena. | T. Omaghomi, and S. Buchberger | ASCE EWRI Congress, Atlanta GA, June 2022 |
| 8 | Extending the Water Demand Calculator to Commercial and Institutional Buildings: A survey of Plumbing Professionals Attending 2021 ASPE Technical Symposium. | T. Omaghomi, NM. Ferretti, G. Klein, and S. Buchberger | ASPE Pipeline, June 15 2022 |
| 9 | Microphone-Based Non-Invasive Sensor Module for Waterflow Event Detection in Premise Plumbing Systems | G. Batra | University of Cincinnati MS Thesis, Aug. 2022 |
| 10 | Battery-powered wireless sensor network for non-invasive monitoring of water usage events in premise plumbing systems | C. Choudhary, G. Batra, T. Wang, T. Omaghomi, S.G. Buchberger, and T. Li | IEEE Sensors 2022 Conference, Dallas, TX, Oct. 2022 |
| 11 | Non-Invasive Calorimetric Sensor for Waterflow Event Detection in Premise Plumbing Systems | C. Choudhary, G. Batra, S. Buchberger, and T. Li | IEEE Sensors 2022 Conference, Dallas, TX, Oct. 2022 |
| 12 | Simulating Plumbing Fixture Probability of Use | T. Omaghomi | WDC Summit, November 2022 (Online) |
| 13 | What Have We Learned About Using the WDC? | Gary Klein | WDC Summit, November 2022 (Online) |
| 14 | Right-Sizing is the 2nd Domino | Gary Klein | 2022 EWTS, San Antonio, May 2023 |
| 15 | Recent Advances in the WDC and Premise Plumbing Modeling Research | S. Buchberger, T. Omaghomi, and T. Li | ASCE EWRI Congress, Nevada, June 2023 |
| 16 | Methods of Calculating the Probability of Fixture Use for Estimating Peak Demand in Buildings | T. Omaghomi, and S. Buchberger | ASCE EWRI Congress, Nevada, June 2023 |

## A.2. Data Collection Template for Nonresidential Buildings

University of CINCINNATI

**Commercial/Institutional Building Water Use Data Submission Template**

### Building Details

Location (City, State):

Building Use: Select Building Item List Other:

Building Floor Area: Select Unit: Choose One

Number of Floors: Number of Water Meters:

Water Meter Size(s):

Total Number of Fixtures in the Building:

Monitoring Point: Select from options List if Other:

Fixture Count Beyond Monitoring Point *(Ignore if entire building is monitored)*:

If Known, Specify Fixture Efficiency/Flowrate: Select or enter choice

***(Add details of fixture type and count <u>beyond monitoring point</u> on page 2)***

### Sampling Details

Recording Frequency (seconds):

Type and Model of Flowmeter:

Sensitivity of Flowmeter:

Start Date: End Date:

Comment(s) or Description of Attached File(s):

### Contact Details

Name:

Company:

Email: Phone:

### Required Data Format

| Date | Time | Flow |
|---|---|---|
| 1/1/2020 | 12:00:00 AM | 0.00 |
| 1/1/2020 | 12:00:05 AM | 0.00 |
| : | : | : |
| 1/10/2020 | 6:59:55 AM | 5.79 |
| 1/10/2020 | 7:00:00 AM | 3.32 |
| 1/10/2020 | 7:00:05 AM | 1.86 |
| 1/10/2020 | 7:00:10 AM | 0.00 |
| : | : | : |
| : | : | : |
| 1/19/2020 | 1:35:30 PM | 2.30 |
| 1/19/2020 | 1:35:35 PM | 3.50 |
| 1/19/2020 | 1:35:40 PM | 3.50 |
| : | : | : |
| 1/19/2020 | 1:36:55 PM | 3.40 |
| 1/19/2020 | 1:37:00 PM | 1.80 |
| 1/19/2020 | 1:37:05 PM | 0.50 |
| : | : | : |
| : | : | : |
| 1/26/2020 | 9:15:30 PM | 1.15 |
| 1/26/2020 | 9:15:35 PM | 1.15 |
| 1/26/2020 | 9:15:40 PM | 1.15 |
| : | : | : |
| 1/26/2020 | 9:16:20 PM | 1.15 |
| 1/26/2020 | 9:16:25 PM | 1.15 |
| 1/26/2020 | 9:16:30 PM | 0.00 |
| : | : | : |
| : | : | : |
| 1/30/2020 | 11:59:50 PM | 1.62 |
| 1/30/2020 | 11:59:55 PM | 0.00 |

Flow Units: Volume ☐ Flow rate ☐

Choose One

Select File Format: .csv ☐ .xlsx ☐ Others ☐

Date Submitted:

RESET FORM

**<u>NOTES:</u>**

- The data supplied should follow the format provided, Date, Time, and Flow information.
- Military time format is acceptable.
- The recording frequency should not exceed 60 seconds. The required data format is shown in 5 seconds.
- For instances with incomplete or missing data, insert -99 or No data.
- Send the completed template and data file(s) (or link to download the data file(s)) to Steven.Buchberger@uc.edu with subject line C/I WATER USE DATA. An option to upload data file can be provided on request.

Page 1 of 2

| List of Typical Commercial Fixtures | | |
|---|---|---|
| **Fixture Type** | **Fixture Count** | **Comments or Specific Fixture Detail** |
| Bar Sinks | | |
| Circular Wash Fountain | | |
| Commercial Clothes Washer | | |
| Commercial Dishwasher | | |
| Commercial Icemaker | | |
| Commercial Water Closet | | Select Type of Water Closet |
| Commercial Water Closet-Other type | | Select Type of Water Closet |
| Drinking Fountain | | |
| Hand Washing Sink** | | |
| Jacuzzi (Hotels) | | |
| Kitchen Sinks*** | | |
| Lavatory Faucets | | |
| Prep Sink (Food Prep) | | |
| 3-Compartment Sink (Food Prep) | | |
| Service Sink/ Mop Basin | | |
| Shower | | Select Type of Shower |
| Urinals | | Select Type of Urinal |
| Other Fixtures (List) | | |
| Other Fixtures | | |
| Other Fixtures | | |
| Other Fixtures**** | | |

** Not inside restrooms, e.g., hospital rooms, nurse stations, restaurant prep areas.
*** In break rooms.
**** Fixture unique to building type such as dental cuspidor, clinical sinks, wall hydrants, commercial garbage disposals, dipper wells, food steamers, combination ovens etc.

**NOTES:**

- The data supplied should follow the format provided, Date, Time, and Flow information.
- Military time format is acceptable.
- The recording frequency should not exceed 60 seconds. The required data format is shown in 5 seconds.
- For instances with incomplete or missing data, insert -99 or No data.
- Send the completed template and data file(s) (or link to download the data file(s)) to *Steven.Buchberger@uc.edu* with subject line C/I WATER USE DATA. An option to upload data file can be provided on request.

Page 2 of 2

## Appendix B. List of Symbols, Abbreviations, and Acronyms

***a***
Fixture activation factor (Dimensionless)

***b***
Fixture busy time (Minutes or seconds)

***ºC***
Unit of measuring temperature (Celsius)

***dBV***
Unit for measuring voltage (Volts)

***GHz***
Unit of measurement for EM waves (Gigahertz)

***H***
Hunter Number is the average number of busy fixtures during the peak demand period (Dimensionless)

***J***
Unit of energy (Joules)

***k***
Number of identical fixtures in a restroom

***m***
Number of water use events at fixtures

***mA***
Unit of measurement for electric current (Milliamp)

***mAh***
Measure of (electric) power over time (Milliamp hours)

***mW***
Unit of power (Milliwatt)

***N***
Number of people entering or departing a restroom under steady conditions

***p***
Probability of water flowing at a fixture (Dimensionless)

$p_c$
Fixture probability of use during congestion (Dimensionless)

***q***
Fixture flowrate (Liters (Gallons) per minute)

***R***
Inter arrival rate (Per time unit)

***t***
Duration of flow at a fixture (Minutes or seconds)

***$t_m$***
Duration of flow for water use event m (Minutes, Seconds)

***T***
Duration of fixture observation (Minutes, Seconds)

***$T_0$***
Duration when a fixture is occupied (Minutes, Seconds)

***U***
Uniform random number between 0 and 1

***V***
Volume of flow per pulse Liters (Gallons)

***V***
Voltage (Volts)

***z***
Standard score in the normal distribution table

***λ***
Arrival rate (Per minute)

***τ***
Duration of flow at fixture per pulse (Minutes, Seconds)

***μ***
Service rate (Per minute)

***ρ***
Utilization factor (Dimensionless)

**ADC**
Analog-Digital Converter

**ARM**
Advanced RISC (*Reduced Instruction Set Computer*) Machine

**ASPE**
American Society of Plumbing Engineers

**AWWA**
American Water Works Association

**BLE**
Bluetooth Low Energy

**CI**
Commercial and Institutional

**CBSC**
California Buildings Standards Commission

**CPC**
California Plumbing Code

**ECM**
Electret Condenser Microphone

**EPAct92**
Energy Policy Act of 1992

**FoM**
Figure of Merit

**GPM**
Gallons per Minute

**IEEE**
Institute of Electrical and Electronics Engineers

**IAPMO**
International Association of Plumbing and Mechanical Officials

**IIR**
Infinite Impulse Response

**MEMS**
Microelectromechanical Systems

**MCU**
Microcontroller Unit

**NBS**
National Bureau of Standards

**NIST**
National Institute of Standards and Technology

**PCB**
Printed Circuit Board

**PER**
Packet Error Rate

**PEX**
Cross-linked Polyethylene Pipe

**PRP**
Poisson Rectangular Pulse

**RF**
Radio Frequency

**RMS**
Root Mean Square

**SM(i)**
Sensor Modality (i)

**SMD**
Surface Mount Device

**SNR**
Signal-to-Noise Ratio

**SSI**
Signal Strength Indicator

**UART**
Universal Asynchronous Receiver-Transmitter

**UC**
University of Cincinnati

**UPC**
Uniform Plumbing Code

**USB**
Universal Serial Bus

**WDC**
Water Demand Calculator

**WSFU**
Water Supply Fixture Units

**WQA**
Water Quality Association